Fuel 427 (2027) 139540

Contents lists available at ScienceDirect

Fuel

journal homepage: www.elsevier.com/locate/fuel

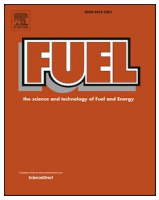

Full Length Article

Levelized cost of CO_2 avoidance of an oxygen blast furnace with top gas recycling, biomass and on-site PV-powered methanation

Manuel Bailera *, Alexander García-Mariaca

Energy and CO_2 Group, Aragon Institute of Engineering Research (I3A), Department of Mechanical Engineering, Escuela de Ingeniería y Arquitectura, Universidad de Zaragoza, María de Luna 3, 50018 Zaragoza, Spain

ARTICLE INFO

Keywords:
Biomass
Ironmaking
Solar
Methanation
Photovoltaics
Blast furnace

ABSTRACT

The decarbonization of the steel industry is critical for achieving global climate targets, as the conventional blast furnace-basic oxygen furnace (BF-BOF) route remains the dominant yet carbon-intensive production method. This study evaluates the practical and economic viability of integrating oxygen blast furnace (OBF) technology with top gas recycling (TGR), biomass pyrolysis, and power-to-gas (PtG) methanation. Using the JFE Steel plant in Chiba, Japan, as a case study, the research specifically examines the impact of relying exclusively on on-site rooftop photovoltaic (PV) systems to achieve electrical self-sufficiency for hydrogen production. Results show that while this integrated configuration theoretically offers emission reductions of 65–70% with unlimited renewable energy, the actual reduction is capped at 46.4% due to the 141 MWp capacity constraint of the available rooftop area. This mitigation is driven primarily by the transition to OBF-TGR mode (15.4 percentage points) and permanent carbon storage (29.2 percentage points), whereas the contributions from biomass and synthetic natural gas (SNG) are limited to 1.8 percentage points. Economic analysis indicates a total CAPEX of 1,320 M€, largely attributed to carbon capture and electrolysis infrastructure. However, the system proves commercially viable under current market trends; a green steel premium of 186 €/t or a combination of CO_2 tax savings and lower premiums can achieve profitability. The Levelized Cost of CO_2 Avoidance (LCCA) is calculated at 126 €/t_{CO2} when no green premium is applied. Ultimately, OBF-TGR integration represents a robust, financially feasible pathway for partial decarbonization and the certification of net-zero steel batches.

1. Introduction

Iron and steel production is essential for modern society, providing multiple applications in construction, transportation, and manufacturing. There exist three main routes for the production of steel: (1) BF-BOF, Blast furnace-basic oxygen furnace route; (2) Scrap-EAF, Scrap-based electric arc furnace; and (3) DRI-EAF, Direct reduced iron-electric arc furnace.

The Scrap-EAF route produces steel by melting recycled scrap using electricity. It represents 23% of the global steel production, but the expansion of this technology is limited because of the scrap availability [1]. The DRI-EAF route is an alternative in which scrap is replaced with direct reduced iron, and it represents 7% of the world steel production. The direct reduced iron contains > 90% metallic iron, and it is produced in combustion-free reactors that reduce the iron ore using natural gas, hydrogen or coal-based syngas [2]. Depending on the share of scrap and DRI, the energy consumption of producing hot metal through these routes varies from 4 to 10 GJ/t_{HM}, and the CO_2 emissions between 300 and 1,300 kg_{CO2}/t_{HM} [1].

The BF-BOF route is the dominant process for steelmaking, accounting for 70% of global production. It consists of a blast furnace, in which the iron ore is reduced by coke to obtain hot metal. Then, the basic oxygen furnace lowers the carbon content of the molten iron to produce the crude steel. This route is highly energy- and carbon-intense, resulting in 13–14 GJ/t_{HM} net energy consumption and 2,000 – 2,200 kg_{CO2}/t_{HM} specific emissions [1].

The ambitious target of the European Union for achieving carbon neutrality by 2050 [3] is increasing the interest in developing low-emission technologies in the steel industry, as it is responsible for 7% of global CO_2 emissions [4]. Since the global steel demand cannot be covered through recycled scrap, the BF-BOF route will maintain its dominance in the market. It is expected that at least 20% of today's blast furnaces will still be in operation by year 2050, because they will only phase-out at relining, what typically takes places every 20 – 40 years [5]. Therefore, innovative methods for CO_2 reduction in blast furnaces must

* Corresponding author.
E-mail address: mbailera@unizar.es (M. Bailera).

https://doi.org/10.1016/j.fuel.2026.139540
Received 16 February 2026; Received in revised form 13 April 2026; Accepted 15 April 2026
Available online 30 April 2026

Nomenclature

Symbols

t	operating hours, h
V	Volume produced/consumed/available, Nm^3
W	Electricity produced/consumed/available, kWh
w	Specific electricity consumption, kWh/Nm^3
$\dot{W}$	Power, kW

Greek symbols

δ	calculation parameter, h
ϵ	conversion efficiency, Nm^3_{SNG}/Nm^3_{H2}
η	efficiency, –
τ	storage capacity in terms of nominal operating hours, h

Subscripts and superscripts

$*$	Nominal load/full capacity
$\#$	Partial load
$-$	Dropped/discarded
1	Interval of 1-hour duration
b	Li-ion battery
e	Electrolyzer
j	Hour j of the year
m	methanation
p	Peak power
PV	Photovoltaic panels
s	H_2 storage/H_2 tank

be developed.

One such method is top gas recycling (TGR), which consist on the recycling of the exhaust gas of the BF back into the process (Fig. 1, b). This gas acts as reducing agent and therefore diminishes the coke consumption. The gas composition is typically 22%–24% CO_2, 20%–25% CO, 0%–2% H_2O, 3%–4% H_2, and 47%–53% N_2, in volume. However, injecting CO_2 or H_2O to the blast furnace is not desirable as they actually increase the fuel consumption and hinders the reduction of iron oxides because of displacing the chemical equilibrium. Therefore, carbon capture (CC) is included before recycling the top gas, in order to reject $\geq$ 90% of the CO_2 [6,7]. The recirculated gas can be injected at tuyeres (lower zone), but also at the shaft (mid zone), at the preparation zone (upper zone), or at a combination of them [4]. The CO_2 reduction achieved by this method is $<$ 15% because of the presence of N_2 in the recirculated gas [8].

The top gas recycling technique, which aimed for valorizing exhaust gases, had similarities with oxy-fuel combustion processes, in the sense that a gas stream is recirculated and a carbon capture stage is needed. Thus, TGR evolved to the possibility of combining it with oxygen blast furnaces (OBF, Fig. 1, c). Oxygen blast furnaces use pure oxygen instead of air to burn coke, reducing the amount of fossil fuel required and resulting in higher energy efficiency. Since part of the blast furnace gas is recirculated in top gas recycling, it palliates the lack of nitrogen during oxy-fuel combustion, keeping similar fluid- and thermo-dynamic behavior than in air-blown combustion. This allows to reduce the coke consumption up to 150 kg/t_{HM} (34% decrease with respect to conventional BF) [4]. Prototype-scale OBF showed 200 – 230 kg/t_{HM} as the minimum feasible coke rate [9]. The decrease in CO_2 emissions is in the range 100 to 500 kg_{CO2}/t_{HM}, which means 10% – 40% reduction with respect to BF [10,11]. Additionally, since CO_2 is rejected from the recycled top gas via a capture stage during recycling, a non-negligible amount of highly-concentrated CO_2 is available for permanent storage [4].

An alternative option to take advantage of the captured CO_2 is to combine OBF with Power to Gas (PtG) [12]. PtG technology consumes renewable electricity to produce H_2 via water electrolysis [13], which is then combined with the CO_2 emissions of the ironmaking process to obtain synthetic natural gas (SNG) [14]. This synthetic fuel is used in the blast furnace to keep carbon in a closed loop and avoid geological storage (Fig. 1, e) [12]. About 70 – 90 kg_{CO2}/t_{HM} could be kept in closed loop and prevented from being permanently stored, which represents 5 – 7% of the emissions of a conventional BF [12]. Therefore, the combination of OBF with PtG might reduce emissions up to 45% with respect to air-blown blast furnaces [12,15]. Moreover, the electrolysis in PtG produces O_2 that can be used in the oxygen blast furnace, therefore diminishing the electricity consumption of the air separation unit that is needed to enriched the hot blast in OBF [16,17]. Depending on how modern the technology of the steel plant is, the ASU consumption may vary between 260 and 400 kWh/t_{O2} [18,19].

An alternative method for CO_2 reduction in blast furnaces is the utilization of biomass resource. In fact, some studies showed that biomass strategies are better than CO_2 capture strategies [20]. Raw biomass could only be considered as a substitute for the pulverized coal that is injected at the tuyeres. However, the poor grindability of raw biomass leads to excessive energy for grinding. In addition, its low energy density means requiring more biomass than coal, what in turn leads to greater ash content in the blast furnace, causing operational problems [21]. The common option adopted to use biomass in ironmaking is the production of biochar, which is the solid product obtained after the torrefaction or pyrolysis of biomass. This process upgrades biomass for ironmaking, reaching similar heating values and ratios on O/C and H/C than those for coal. Still, the low mechanical strength of biochar is not sufficient to support the burden inside the furnace, so it can only replace around 10% of the coke that is introduced at the top. Hence, the injection of pulverized biochar at the tuyeres, to replace the pulverized coal injection, is the solution adopted by the industry (Fig. 1, d). Typical injections rates of biochar are 100 – 150 kg/t_{HM}. Depending on the quality of the biochar, the CO_2 reductions vary from 17% to 30% for this technology [21]. Some authors proposed to co-inject the biochar and the syngas from pyrolysis process in order to increase the biomass utilization [21].

At this point, further CO_2 reductions required the integration of some of the techniques mentioned. Thus, Bailera et al. proposed the combination of biomass utilization and power to gas in oxygen blast furnaces (Fig. 1, f) [15]. This novel system was assessed for different pyrolysis temperatures, what translates into different syngas compositions entering in the methanation process. The best configuration found was for pyrolysis at 700 °C, reaching 58% CO_2 reduction in the blast furnace emissions.

Currently, the most novel proposal found in literature is the integration of all the mentioned alternatives for CO_2 reduction in blast furnace: TGR, OBF, PtG, and biomass pyrolysis (Fig. 1, g). Different technical limitations may apply on this type of integration, what in turn affects the amount of biomass, auxiliary fuels or TGR used, and therefore to the potential for CO_2 reduction. In the analysis of Legaz et al. [22], the biomass and PtG parts were constrained by the limitation of 220 kg/t_{HM} of biochar injection [23], while the TGR part was constrained by the requirement of consuming at least 190 kg/t_{HM} of coke (for mechanical stability) [9]. Under these conditions, the CO_2 emissions can be reduced by 65% to 70% with respect to conventional blast furnaces. A summary of all the decarbonization strategies is presented in Table 1 and Fig. 1.

Considering the recent advances in blast furnace decarbonization systems, the novelty of this article relays on evaluating the integration of the option with the greatest potential for emission reduction in a real steel plant located in Japan (Fig. 1, g). Unlike previous assessments of OBF-TGR and Power to Gas integration that rely on theoretical renewable energy supplies, this study introduces a land-constrained methodological framework. The novelty lies in quantifying the impact of utilizing exclusively on-site available surfaces (rooftops) for PV generation within a brownfield steel plant. This approach shifts the focus from 'maximum technical potential' to 'realistic implementation capacity', providing a more robust benchmark for industry transitions where land

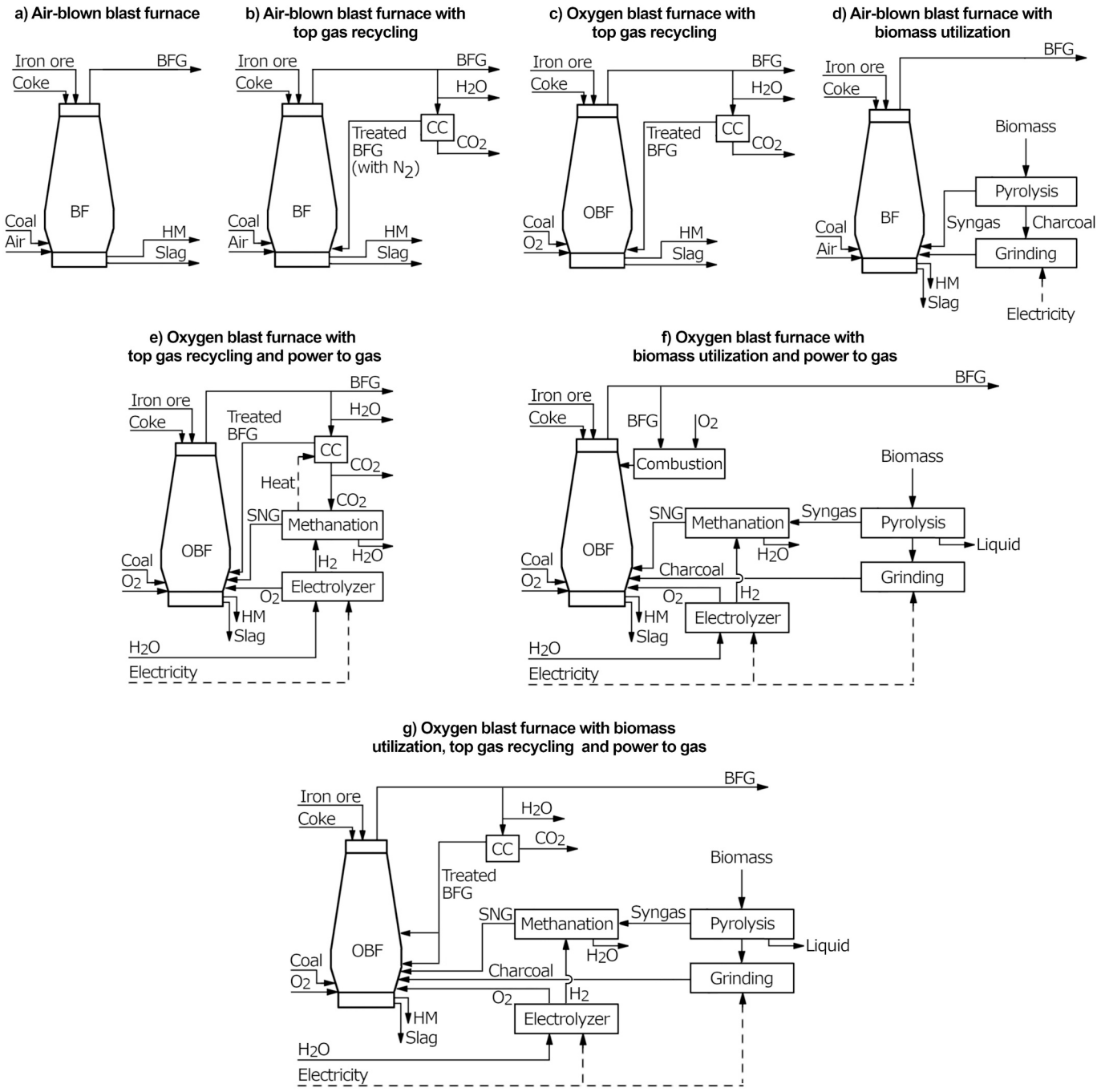

Fig. 1. Process flow diagram of conventional blast furnace *(a)*, and different strategies for decarbonization *(b – g)*.

Table 1
Summary of decarbonization strategies for blast furnaces.

Decarbonization strategy	TGR	OBF	PtG	Biomass	Diagram	CO_2 reduction	Ref.
Air-blown BF with TGR	✓	×	×	×	Fig. 1b	< 15%	[8]
Oxygen BF with TGR	✓	✓	×	×	Fig. 1c	10% – 40%	[10,11]
Oxygen BF with TGR and PtG	✓	✓	✓	×	Fig. 1e	20% – 45%	[12,15]
Air-blown BF with biomass utilization	×	×	×	✓	Fig. 1d	17% – 30%	[15,21]
Oxygen BF with biomass utilization and PtG	×	✓	✓	✓	Fig. 1f	45% – 60%	[15]
Oxygen BF with biomass utilization, TGR and PtG	✓	✓	✓	✓	Fig. 1g	65% – 70%	[22]

availability and grid dependency are major bottlenecks. These realistic studies have been performed previously for lime kilns in ironmaking plants but not for blast furnaces [24]. The study examines the effective CO_2 reduction under the specific assumption that the plant relies exclusively on renewable electricity generated by photovoltaic (PV) panels installed on its own buildings when it comes to produce the hydrogen for methanation. This approach makes it possible to analyze the decarbonization capacity while preserving the steel plant's electrical

independence. The analysis is further complemented by an economic assessment of the proposed integration. No studies on this type of integration are found in literature, to the authors knowledge. Furthermore, the developed framework provides a transferable assessment tool for other brownfield steelworks. It shifts the focus from theoretical decarbonization to a realistic, land-constrained evaluation that is applicable to any industrial site with limited expansion area for renewable infrastructure.

2. Case study

The selected case study is the steelmaking plant of JFE Steel in Chiba, Japan. JFE Steel is one of the largest steel producers in the world and has established strong decarbonization plans in order to reduce emissions by 30% by the year 2030 and become carbon neutral by 2050. The process flow diagram to be analyzed consists of an oxygen blast furnace (OBF) with top gas recycling (TGR), biomass utilization, and Power-to-Gas (PtG) (Fig. 2). The PV panels for H_2 production, which is required in the integration concept, are set to be installed in the roof of the different buildings of the steelworks. In the absence of solar-generated electricity for H_2 production, the integration is limited exclusively to the OBF with TGR. When H_2 is available, it is utilized to methanate the syngas derived from biomass pyrolysis. Consequently, the resulting synthetic natural gas (SNG) replaces fossil natural gas, while the pyrolysis charcoal is used as a substitute for coal. The volume of available PV power determines the amount of syngas that can be processed and, therefore, the quantity of biomass to be pyrolyzed. This, in turn, dictates the substitution ratios of fossil fuels. The integrated system is evaluated against a reference case consisting of a conventional air-blown blast furnace.

3. Methodology

3.1. Sizing and management of the PV solar field

The buildings for PV installation were identified using satellite images from Google Earth (Fig. 3) [25]. Thus, by observing the position of chimneys, the presence of emissions, as well as the orientation of rooftops and shadows, the rooftops were classified according to their condition as follows:

- Type 1: Large roof surfaces suitable for the installation of solar panels, with little impact from the surrounding conditions (shadows, dust, etc.).

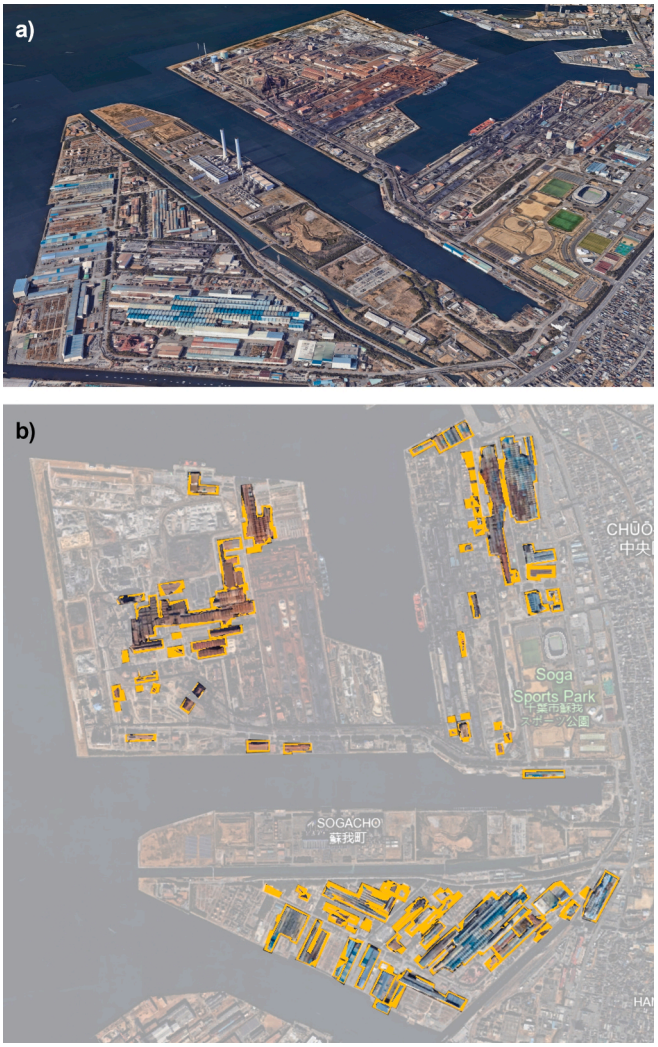

Fig. 3. A) satellite image for jfe steel site in chiba, japan (35° 34′ 23″ N, 140° 05′ 41″ E), and b) roof area [25].

- Type 2: Roofs that, due to their location, size, or surface condition, raise doubts about the technical and/or economic feasibility of their

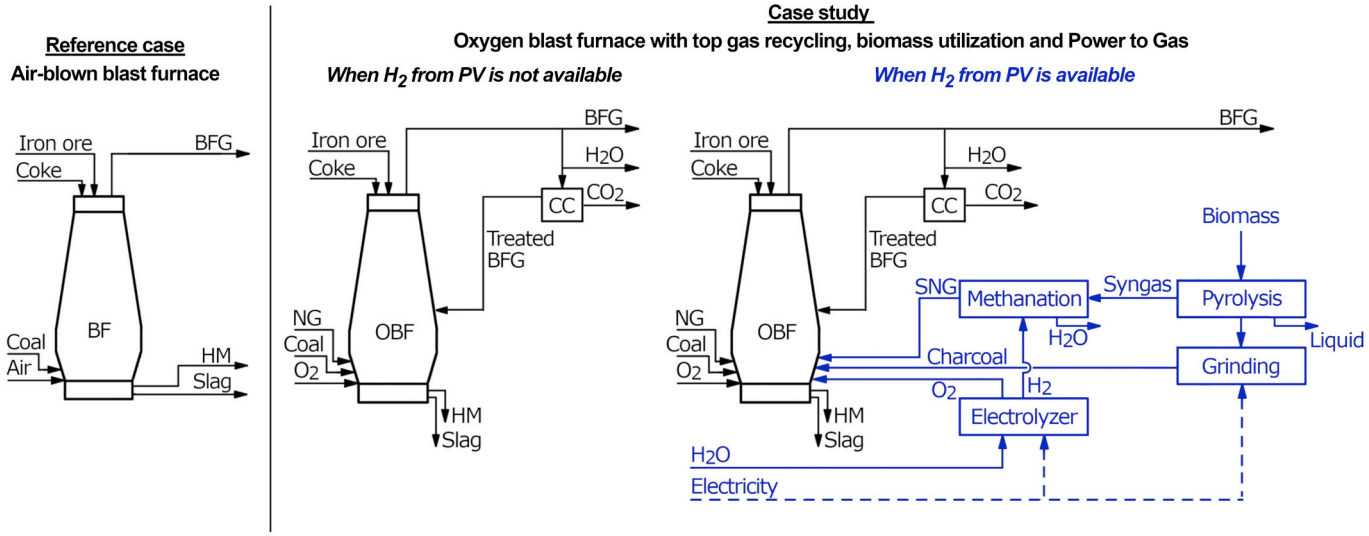

Fig. 2. Process flow diagram of the reference case (air-blown blast furnace) and of the case study (OBF with TGR, biomass and PtG).

Table 2
Location and technical data of the PV solar field.

Parameter	Data
Location	Chiba, Japan
Latitude (dec)	+35.57
Longitude (dec)	+140.09
Type 1 roof	
N° buildings	46
Roof area (m^2)	938,889
Type 1 + Type 2 roof	
N° buildings	109
Roof area (m^2)	1,107,180
PV technology	Crystalline silicon
PV system loss (%)	20
PV panel efficiency (%)	15
PV panel slope (°)	36

use. This category also includes surfaces where the presence of emissions or shadows from nearby towers or chimneys makes solar panel installation not recommended.

It was decided to proceed only with the buildings classified as Type 1 as available for panel installation, since the investment required for installing panels on Type 2 buildings was considered too risky (Table 2).

The electricity production from the PV panels was calculated through the PVGIS tool from the European Commission (version 5.2), using the PVGIS-SARAH3 data base [26]. The mounting type was assumed fixed, and the slope and azimuth of the panels were optimized by the PVGIS tool. The PV technology was crystalline silicon, and the system loss was fixed at 20%, which is higher than the default value of 14% because of the expected ambient dust in the steelworks (it must be noted that this loss does not include losses related to the angle of incidence and temperature, which are already estimated and taken into account by the PVGIS tool according to the satellite data). The data on electricity production were retrieved in an hourly basis for 1 kWp of power capacity at latitude + 35.57 and longitude + 140.09. This electricity production was then scaled up to the total peak power that can be installed in the available solar area by assuming 15% efficiency [27,28] of the PV panels (Eq.(1)) [29].

$$\text{Peak power}\,[\text{kWp}] = \text{Solar area}\,\left[\text{m}^2\right] \times \text{PV panel efficiency}\,[-] \tag{1}$$

Additionally, a Li-ion battery was included to mitigate variations in the electricity production from the PV panels, which might occur due to cloud coverage. The nominal power of the battery ($\dot{W}_b^*$) was assumed to be 5% of the total peak power of the PV solar field ($0.05\dot{W}_{PV,p}^*$) [30], the efficiency of the battery (η_b) was set at 85% [31,32], and its energy capacity equal to 4 h of nominal operation (τ_b) [30,31]. The electricity available in the Li-on battery at hour j ($W_{b,j}$) depends on the PV electricity production ($W_{PV,j-1}$) and the charge of the battery ($W_{b,j-1}$) at the preceding hour $j-1$, and on the electrolyzer consumption at nominal load for 1 h ($W_{e,1}^*$) (Eq.(2)).

$$W_{b,j} = \begin{cases} W_b^* & \text{if } W_{PV,j-1} \geq W_{e,1}^* \text{ and } \left(\left(W_{PV,j-1} - W_{e,1}^*\right)\eta_b + W_{b,j-1}\right) \geq W_b^* \\ \left(W_{PV,j-1} - W_{e,1}^*\right)\eta_b + W_{b,j-1} & \text{if } W_{PV,j-1} \geq W_{e,1}^* \text{ and } \left(\left(W_{PV,j-1} - W_{e,1}^*\right)\eta_b + W_{b,j-1}\right) < W_b^* \\ \left(W_{PV,j-1} + W_{b,j-1}\right) - W_{e,1}^* & \text{if } W_{PV,j-1} < W_{e,1}^* \text{ and } \left(W_{PV,j-1} + W_{b,j-1}\right) \geq W_{e,1}^* \\ 0 & \text{if } W_{PV,j-1} < W_{e,1}^* \text{ and } \left(W_{PV,j-1} + W_{b,j-1}\right) < W_{e,1}^* \end{cases} \tag{2}$$

It should be noted that the available electricity in the battery is accounted after losses. At full capacity (W_b^*), it is equal to its nominal power capacity ($\dot{W}_b^*$) multiplied by the equivalent hours of energy storage (τ_b), accounting for losses (i.e., $W_b^* = \tau_b \eta_b \dot{W}_b^*$).

3.2. Sizing and management of the power to gas plant

The electricity consumed by the electrolyzer, $W_{e,j}$, was computed through Eq.(3) by knowing both the electricity produced by the PV panels, $W_{PV,j}$ (data from PVGIS scaled by Eq.(1)), and the electricity provided by the Li-ion battery ($W_{b,j}$, Eq.(2)). In Eq.(3), $W_{e,1}^*$ is the nominal electricity consumption of the electrolyzer in 1 h ($W_{e,1}^* = 1 \cdot \dot{W}_e^*$).

$$W_{e,j} = \begin{cases} W_{e,1}^* & \text{if } W_{PV,j} \geq W_{e,1}^* \\ W_{e,1}^* & \text{if } W_{PV,j} < W_{e,1}^* \text{ and } \left(W_{PV,j} + W_{b,j}\right) \geq W_{e,1}^* \\ W_{PV,j} + W_{b,j} & \text{if } \left(W_{PV,j} + W_{b,j}\right) < W_{e,1}^* \end{cases} \tag{3}$$

In order to select $W_{e,1}^*$ (i.e., the size of the electrorlyzer), it was used the load duration curve (LDC) (Fig. 4). This curve relates the nominal operating load of the electrolyzer ($\dot{W}_e^*$) with the maximum operating hours that it might work at that load ($t_{\dot{W}_e^*}$, Eq.(4)). The product of the two values ($\dot{W}_e^* \cdot t_{\dot{W}_e^*}$) is a measure of the electrical energy that could be processed by the electrolyzer at nominal load (W_e^*, gray area in Fig. 4).

$$t_{\dot{W}_e^*} = \sum_j \delta_j \quad \text{where} \quad \delta_j = \begin{cases} 0 & \text{if } W_{e,j} < W_{e,1}^* \\ 1 & \text{if } W_{e,j} = W_{e,1}^* \end{cases} \tag{4}$$

The main criterion (criterion 1) for selecting the nominal power

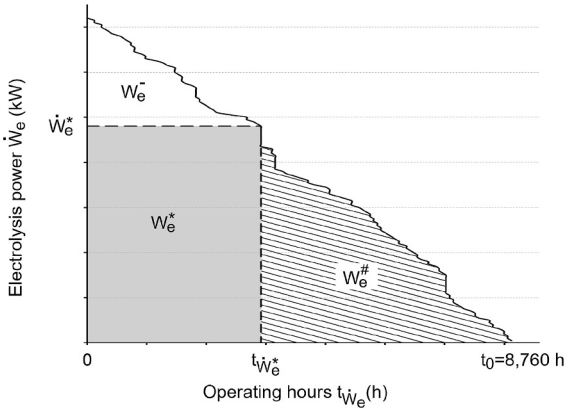

Fig. 4. Load duration curve methodology (blank area: energy discarded; gray area: energy processed at nominal load; pattern area: energy processed at partial load).

capacity of the electrolyzer was to maximize the energy processed at nominal load (i.e., maximization of W_e^*, the grey area under the LDC, in Fig. 4) [33]. In some cases, large variations in the selected nominal load (e.g., $\dot{W}_e^* \pm 15\%$) only produced small changes in the energy processed at nominal load ($W_e^* \pm 0.1\%$), although the total energy processed remarkably changed ($(W_e^* + W_e^\#) \pm 6\%$). Hence, in these cases, a second criterion (criterion 2) was added to avoid ambiguity: the nominal load derived from the maximization process was increased by progressively decreasing W_e^* at −0.25% intervals until the relative increment in the total processed energy dropped below 1%. Graphically, this means that the grey area (W_e^*) was diminished at −0.25% intervals by increasing $\dot{W}_e^*$ in Fig. 4, until the total area composed by $W_e^* + W_e^\#$ stopped increasing beyond 1% in a single step. This way, we had an electrolyzer with a very similar operational optimization (nearly the same amount of energy processed at nominal load), but with a notable greater total energy processed (i.e., the blank area of discarded energy W_e^- notably decreased, the pattern area of energy processed at partial load $W_e^\#$ increased in the same amount, and the grey area of energy processed at nominal load W_e^* barely changed).

The amount of H_2 produced by the electrolyzer was calculated by Eq. (5), being directly dependent on the electricity consumed. The specific consumption, w_e, was set at 4.5 kWh/Nm^3, corresponding to a commercial containerized PEM electrolyzer in the MW scale [34].

$$V_{H_2,e,j} = W_{e,j}/w_e \tag{5}$$

This H_2 was either sent to storage or to methanation. The H_2 available in the tank at each hour was calculated by Eq.(6), as the sum of the H_2 produced by the electrolyzer ($V_{H_2,e,j-1}$) plus the H_2 already available in the tank ($V_{H_2,s,j-1}$), minus the H_2 consumed by the methanator ($V_{H_2,m,j-1}$), at the previous hour. Then, the H_2 consumed by methanation was calculated by Eq.(7), corresponding to the H_2 available ($V_{H_2,e,j} + V_{H_2,s,j}$) or to the limit of the methanator ($V^*_{H_2,m,1}$).

$$V_{H_2,s,j} = V_{H_2,e,j-1} + V_{H_2,s,j-1} - V_{H_2,m,j-1} \tag{6}$$

$$V_{H_2,m,j} = \begin{cases} V^*_{H_2,m,1} & if\ (V_{H_2,e,j} + V_{H_2,s,j}) \geq V^*_{H_2,m,1} \\ V_{H_2,e,j} + V_{H_2,s,j} & if\ (V_{H_2,e,j} + V_{H_2,s,j}) < V^*_{H_2,m,1} \end{cases} \tag{7}$$

The Eq.(6) assumes no limit for the H_2 storage, so the size required for the H_2 tank would be $\max_j(V_{H_2,s,j})$. This value is completely dependent on the methanation size ($V^*_{H_2,m,1}$) through Eq.(7), which determines the H_2 consumed in methanation, and therefore the surplus sent to the tank. The smaller the methanation plant, the larger the H_2 tank and the higher the capacity factor of the methanation plant. Larger tanks are unsuitable for techno-economic viability, while higher capacity factors are suitable for steady operation. Hence, we minimized the methanation plant size in order to increase its equivalent operating hours, but at the same time it was constrained by the criterion: $\max_j(V_{H_2,s,j}) \leq 66,740$ (constrained minimization solver). This limit is intended for a storage of 6,000 kg of H_2 (i.e., 66,740 Nm^3), which corresponds to the H_2 storage installed in Puertollano (Spain) by Iberdrola, at a 100 MW PV solar plant aimed for the production of green H_2. The H_2 is stored at 60 bar in 11 tanks of 133 m^3 each (23.5 m in height, 2.8 m in diameter and 4.5 cm in thickness) [30]. In the Japanese industrial context, where land for large-scale pressurized storage is limited, this 6,000 kg constraint represents a compact, high-pressure buffering solution that balances system

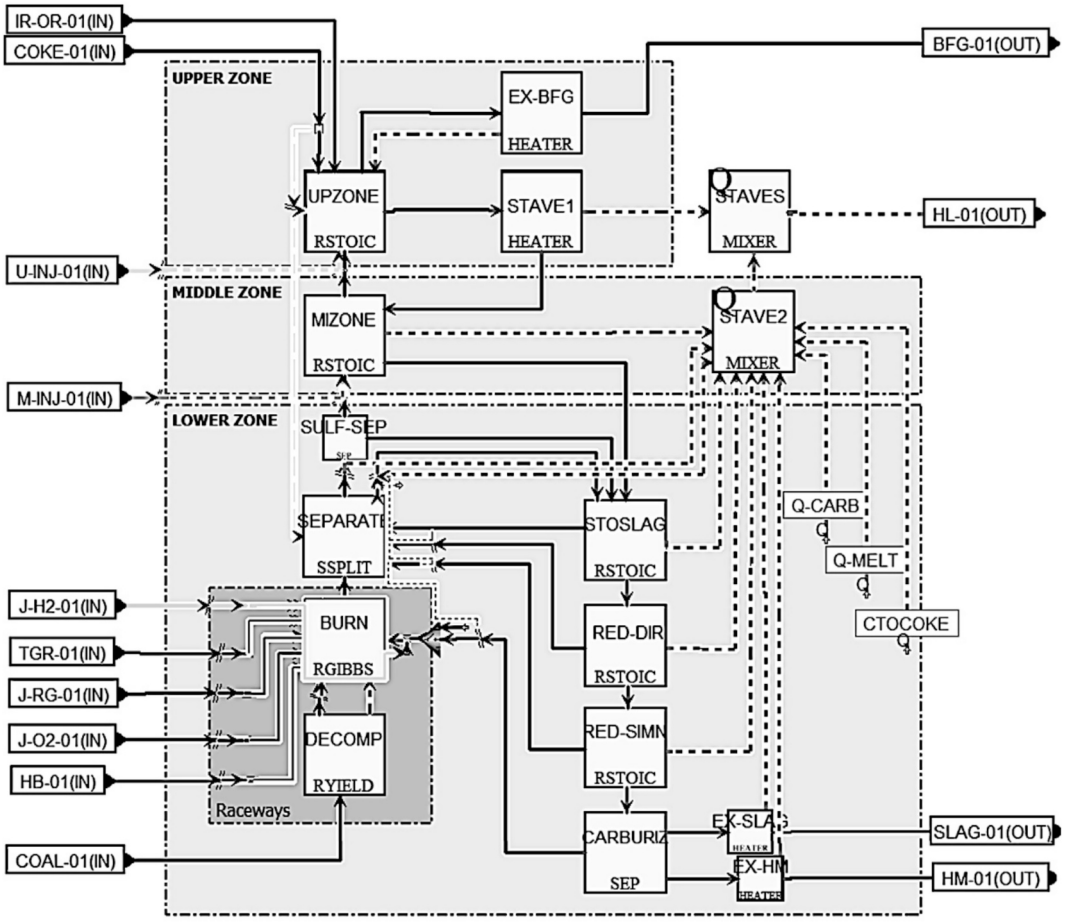

Fig. 5. Process flow diagram of the blast furnace in Aspen Plus.

autonomy with the footprint limitations of a brownfield site.

The SNG production (Eq.(8)) will depend on the composition of the syngas used in methanation, through variable $\epsilon_{m,i}$ (gas conversion efficiency).

$$V_{SNG,m,j} = \begin{cases} V^*_{H_2,m,1}\epsilon_m & if\ (V_{H_2,e,j} + V_{H_2,s,j}) > V^*_{H_2,m,1} \\ (V_{H_2,e,j} + V_{H_2,s,j})\epsilon_m & if\ (V_{H_2,e,j} + V_{H_2,s,j}) \leq V^*_{H_2,m,1} \end{cases} \quad (8)$$

The parameter $\epsilon_{m,i}$, which quantifies the amount of SNG produced per H_2 consumed, was calculated in Aspen Plus by simulating the methanation plant.

3.3. Sizing and management of the pyrolysis plant

The syngas plant is dimensioned to ensure continuous availability for the methanation process. Consequently, production capacity (Eq.(9)), combined with strategic storage (Eq.(10)), must be sufficient to meet total methanation demand (Eq.(11)). The production changes from nominal capacity, V^*_{syn}, to minimum partial load (80%), or shutdown. The tank capacity, $V^*_{syn,s}$, is assumed 150,000 Nm^3 (typical for buffering gases in steelworks at ambient pressure).

The syngas production decision tree has 9 different possibilities (Eq. (9)). The first 8 take place if the available storage space is sufficient, while the ninth occurs if it is about to fill up (at which point production stops). When space is available, a distinction is made between the situation in which the tank is filling (the first 3 cases) and when it is emptying (cases 5 to 8). If the tank level is unchanging (case 4), production remains constant, equal to the previous hour. If the tank is in the process of filling, production varies between 80 and 100% of the nominal capacity, depending on the methanation demand and how empty the tank is (the goal is for the tank not to fill so quickly, so that the pyrolysis plant can operate for more hours, even if at partial load). In cases 5 to 8, in which the tank is discharging, production depends on whether the pyrolysis plant is in operation or not (if it is on, it will continue producing even if the tank is discharging, and if it is off, it will not start producing until the tank is practically empty).

Table 3
Summary of model input and output data regarding the streams crossing the boundary of the blast furnace.

Stream	Description	Flow	Composition	Temperature
IR-OR-01	Iron ore	Input	Input	Input
COKE-01	Coke	Output	Input	Input
HB-01	Air + moisture	Output	Input	Input
COAL-01	Pulverized charcoal injection at tuyeres	Input	Input	Input
J-O2-01	O_2 injection for enrichment at tuyeres	Input	Input	Input
J-H2-01	H_2 injection at tuyeres	Input	Input	Input
J-RG-01	Gas injection at tuyeres	Input	Input	Input
TGR-01	Top gas recirculation injected at tuyeres	Input	Input	Input
M−INJ−01	Gas injection at mid shaft	Input	Input	Input
U-INJ-01	Gas injection at upper part	Input	Input	Input
HM-01	Hot metal	Output	Input	Input
SLAG-01	Slag	Output	Output	Input
BFG-01	Blast furnace gas	Output	Output	Output
HL-01	Heat removed by the staves	Input	–	–

(1.58 Nm^3_{syn}/Nm^3_{SNG} in our study).

3.4. Modelling the integrated concept for blast furnace decarbonization

The blast furnace model is built upon the extended operating line methodology, a recent development by Bailera et al. [35]. This methodology serves as a generalization of the operating line initially proposed by Rist in 1967 [12,36]. It enables the prediction of blast furnace behaviour when operating conditions are altered, even in scenarios involving oxy-fuel regimes and multiple gas and solids injections at different zones. The model's ability to accurately replicate the thermochemical state of the furnace and the operating-line shifts has been thoroughly benchmarked in our previous studies [12,35].

The implementation of the extended operating line methodology is carried out in Aspen Plus, with individual models for the upper, mid, and lower zones of the blast furnace, the latter encompassing the raceways (see Fig. 5). The model involves 10 inlet mass streams, three outlet mass streams, and one outlet heat stream that traverse the blast furnace boundary. It calculates the mass flow of coke, air, hot metal, slag, and blast furnace gas as a function of the temperature of the thermal reserve

$$V_{syn,j} = \begin{cases} 0.8V^*_{syn} & \text{if } V_{syn,s,j-1} < \left(V^*_{syn,s} - V^*_{syn}\right) \text{ and } V_{syn,s,j-1} > V_{syn,s,j-2} \text{ and } V_{syn,m,j} \leq 0.8V^*_{syn} \\ 0.8V^*_{syn} & \text{if } V_{syn,s,j-1} < \left(V^*_{syn,s} - V^*_{syn}\right) \text{ and } V_{syn,s,j-1} > V_{syn,s,j-2} \text{ and } V_{syn,m,j} > 0.8V^*_{syn} \text{ and } V_{syn,s,j-1} > 0.2V^*_{syn} \\ V^*_{syn} & \text{if } V_{syn,s,j-1} < \left(V^*_{syn,s} - V^*_{syn}\right) \text{ and } V_{syn,s,j-1} > V_{syn,s,j-2} \text{ and } V_{syn,m,j} > 0.8V^*_{syn} \text{ and } V_{syn,s,j-1} \leq 0.2V^*_{syn} \\ V_{syn,j-1} & \text{if } V_{syn,s,j-1} < \left(V^*_{syn,s} - V^*_{syn}\right) \text{ and } V_{syn,s,j-1} = V_{syn,s,j-2} \\ 0.8V^*_{syn} & \text{if } V_{syn,s,j-1} < \left(V^*_{syn,s} - V^*_{syn}\right) \text{ and } V_{syn,s,j-1} < V_{syn,s,j-2} \text{ and } V_{syn,j-1} > 0 \text{ and } V_{syn,s,j-1} > 0.2V^*_{syn} \\ V^*_{syn} & \text{if } V_{syn,s,j-1} < \left(V^*_{syn,s} - V^*_{syn}\right) \text{ and } V_{syn,s,j-1} < V_{syn,s,j-2} \text{ and } V_{syn,j-1} > 0 \text{ and } V_{syn,s,j-1} \leq 0.2V^*_{syn} \\ 0 & \text{if } V_{syn,s,j-1} < \left(V^*_{syn,s} - V^*_{syn}\right) \text{ and } V_{syn,s,j-1} < V_{syn,s,j-2} \text{ and } V_{syn,j-1} \leq 0 \text{ and } V_{syn,s,j-1} > V^*_{syn} \\ V^*_{syn} & \text{if } V_{syn,s,j-1} < \left(V^*_{syn,s} - V^*_{syn}\right) \text{ and } V_{syn,s,j-1} < V_{syn,s,j-2} \text{ and } V_{syn,j-1} \leq 0 \text{ and } V_{syn,s,j-1} \leq V^*_{syn} \\ 0 & \text{if } V_{syn,s,j-1} \geq \left(V^*_{syn,s} - V^*_{syn}\right) \end{cases} \quad (9)$$

$$V_{syn,s,j} = V_{syn,j} + V_{syn,s,j-1} - V_{syn,m,j} \quad (10)$$

$$V_{syn,m,j} = V_{SNG,m,j}\nu_m \quad (11)$$

The parameter ν_m quantifies the syngas consumption per SNG produced

zone, chemical efficiency, heat removed by the staves (in both the preparation and elaboration zones), and the inputs specified in Table 3. The blocks and manipulators, with the specified chemical reactions are provided in Table 4 and Table 5. Moreover, to accurately represent the co-processing of traditional pulverized coal and biomass-derived biochar, the simulation architecture was modified to handle two independent solid streams. This allows for the differentiation of the chemical compositions and enthalpy balances of each fuel type during the injection process. By avoiding the common simplification of 'equivalent fuel properties,' the model provides a more robust prediction of the OBF's response to varying biomass substitution ratios. Detailed descriptions of the model can be found in the author's previous papers [35,37].

This Aspen Plus model is the basis to simulate the blast furnace integration of Fig. 2. To this model, the methanation plant is added. The methanation plant is based on the technology developed by Hitachi Zosen Corporation. Their technology comprised two shell-and-tube typed exchange reactors, operating at 5 bar and 250 °C, with an intermediate condensation stage. The final CH_4 content of the synthetic natural gas was 98.5 vol%, and the H_2 content was 1.3 vol%, in dry basis [38]. The corresponding Aspen Plus model (Fig. 6) consisted of two 2-stage compressors for the inlet syngas and H_2 (compression ratios of 2.5:1 and 2:1, with intermediate cooling at 60 °C), two RGibbs equilibrium reactors for the methanation stages (at 250 °C and 5 bar), two Flash reactors for water condensation after each methanator (at 50 °C and 35 °C), and two preheating exchangers before each methanator (at 250 °C).

Regarding the pyrolysis process, it is not affected by upstream equipment. Thus, the Aspen Plus model does not include the blocks of

Table 4
Main blocks of the Aspen Plus simulation.

Block	Type	Process and reactions	Manipulator
UPZONE	Stoichiometric reactor	$3Fe_2O_3 + CO \rightarrow 2Fe_3O_4 + CO_2$ $Fe_3O_4 + CO \rightarrow 3FeO + CO_2$ $CO_2 + H_2 \rightarrow CO + H_2O$	CHEM-EFF UPA
EX-BFG	Heater	It sets the outlet temperature of the blast furnace gas, and returns the excess heat to the upper zone.	UPB
STAVE1	Heater	It sets the temperature at TRZ for the solids descending to the mid zone, and provides the excess heat to the staves.	–
MIZONE	Stoichiometric reactor	$Fe_3O_4 + CO \rightarrow 3FeO + CO_2$ $FeO + CO \rightarrow Fe + CO_2$ $CO_2 + H_2 \rightarrow CO + H_2O$	YDR XR
STAVE2	Q-Mixer	It gathers all the heat streams of the mid and lower zone and provides the net value to the staves.	–
STAVES	Q-Mixer	It gathers the net heat streams of the upper, mid and lower zone. The output is the total heat removed by the staves.	–
SULF-SEP	Separator	It diverts the Sulphur to the block STOSLAG.	–
SEPARATE	Splitter	It gathers all the gases produced in the lower part and the ashes from coal combustion. It separates the gases (sent upwards to the mid zone) and the solids (sent downwards).	–
BURN	Gibbs reactor	It calculates the chemical equilibrium for combustion and the flame temperature.	–
DECOMP	Yield reactor	It decomposes the coal (non-conventional solid) into C, H_2, O_2, N_2, S, SiO_2, Al_2O_3 and CaO to perform calculations.	COMBUST
STOSLAG	Stoichiometric reactor	$Fe + S \rightarrow FeS$ $FeS + CaO + C \rightarrow Fe + CaS + CO$	–
RED-DIR	Stoichiometric reactor	$FeO + C \rightarrow Fe + CO$	–
RED-SIMN	Stoichiometric reactor	$SiO_2 + 2C + 3Fe \rightarrow Fe_3Si + 2CO$ $MnO + C \rightarrow Mn + CO$	HM-SI HM-MN
CARBURIZ	Separator	It separates solids into slag (SiO_2, Al_2O_3, CaO, MgO, MnO, CaS) and hot metal (Fe, C, Fe_3Si, Mn). The remaining C is sent to the burner.	HM-C
EX-SLAG	Heater	It sets the outlet temperature of the slag.	–
EX-HM	Heater	It sets the outlet temperature of the hot metal.	–

Table 5
Manipulators of the Aspen Plus simulation.

Manipulator	Type	Description	Modifies
CHEM-EFF	Design spec	It modifies the extent of Fe_3O_4 reduction according to the chemical efficiency, in order to set the oxidation state of the burden descending to the mid zone equal to Y_R (extended operating diagram).	UPZONE
UPA	Design spec	It modifies the extent of reverse water–gas shift reaction according to the heat removed by the staves in the upper zone. The temperature of the BFG is assumed to be known (when UPA is used, UPB is deactivated).	UPZONE
UPB	Design spec	It modifies the outlet temperature of the BFG according to the heat removed by the staves in the upper zone. The H_2 utilization is assumed to be known (when UPB is used, UPA is deactivated).	EX-BFG
YDR	Design spec	It modifies the extent of FeO reduction in the mid zone according to the percentage of indirect reduction calculated by the RIST block.	MIZONE
XR	Design spec	It modifies the extent of reverse water–gas shift reaction in the mid zone according to the chemical efficiency and the equilibrium of the Fe-O–H system at T_R.	MIZONE
COMBUST	Calculator	It calculates the mass flow of C, H_2, O_2, N_2, S, SiO_2, Al_2O_3 and CaO obtained after the decomposition of the coal, as a function of the ultimate analysis, the moisture and the ash composition.	DECOMP
HM-SI	Design spec	It modifies the extent of SiO_2 reduction according to the composition of the hot metal.	RED-SIMN
HM-MN	Design spec	It modifies the extent of MnO reduction according to the composition of the hot metal.	RED-SIMN
HM-C	Design spec	It modifies the C diverted to HM-01 stream according to the composition of the hot metal.	CARBURIZ
QMELT	Design spec	It sets the heat used for melting the hot metal and slag according to their mass flow and composition.	Q-MELT
QCARB	Design spec	It sets the heat used for carburization according to the C content in the hot metal.	Q-CARB
QCTOCOKE	Design spec	It sets the heat required to consider C as coke instead as graphite in the energy balances, as a function of the mass flow of coke entering the blast furnace. Aspen provides C as graphite by default.	CTOCOKE
RIST	Calculator	It calculates the mass flow of coke and hot blast (air + moisture) according to the extended operating line methodology.	COKE-01, HB-01

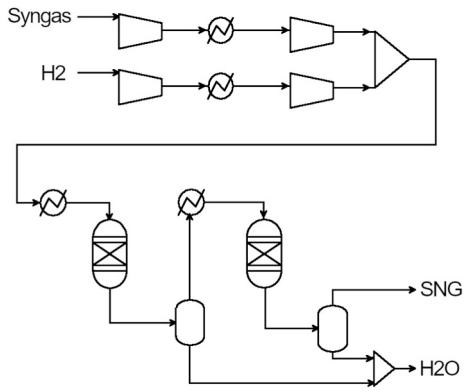

Fig. 6. Process flow diagram of the methanation plant in Aspen Plus.

pyrolysis and grinding but considers the charcoal and the syngas as inputs to the model. The pyrolysis process is assumed at 700 °C, according to previous studies (details in biomass, charcoal and syngas composition and yields can be found in [15]). Regarding carbon capture, it is assumed a 90% carbon capture ratio, with a 2.67 MJ/kg_{CO2} energy penalty [39]. The thermal energy required for solvent regeneration is supplied through the recovery of waste heat from the integrated plant, particularly from the cooling of the recycled top gas and the exothermic methanation process.

A distinction is made between CO_2 generated by the Blast Furnace based on its final destination: a portion is permanently stored via Top Gas Recycling, while the remainder is emitted into the atmosphere. Within the latter, a specific fraction is classified as carbon–neutral, corresponding to the use of biomass-based sources such as charcoal or SNG. Total final emissions account for the Blast Furnace Gas released, adjusted for net-zero biogenic contributions and the eventual conversion of CO into CO_2 during combustion.

3.5. Methodology for techno-economic analysis

The economic analysis follows a 'factored estimated' methodology, which is based on the knowledge of major items of equipment (this methodology has a typical accuracy of ± 30%). The CAPEX comprises the PV panels, the electrolyser, the H_2 storage tank, the pyrolysis plant, the methanation plant, the amine scrubbing and the air separation unit, as well as other direct and indirect costs (Table 6). The OPEX considers the catalyst renovation for methanation, the amine renovation, the required water, the biomass, and the operation and maintenance. The incomes are the savings in fossil natural gas and coal, and the benefits from green premium for steel. The latter follows the Mass Balance Approach, which concentrates the yearly-round CO_2 savings into a specific "Green Steel" batch. The loan amortization is 20 years, with 8000 h per year of operation [40].

4. Results and discussion

4.1. Renewable electricity and H_2 production

Following the methodology described previously, the PV field was sized as a function of the available roof area (Table 7). Then, the electrolyzer was sized as a function of the load duration curve. Therefore, the results regarding the electricity and H_2 production were independent of the size and management of the methanation and pyrolysis plants.

The total solar area for the buildings that are ready for PV installation was 0.94 km^2, which was the equivalent to 140.8 MWp of PV capacity. With this installation size, the yearly electricity production of the PV field was 185 GWh, presenting 1313 equivalent operating hours (Table 7). The auxiliary Li-ion batteries that were installed had a round-trip electricity storage capacity of 23.9 MWh (4 h × 7.04 M × W0.85).

Table 6
Equations for the economic analysis.

	Cost equation	Parameters α, β, γ	Ref.
CAPEX (M€)			
Amine Plant	$0.06772 \cdot \alpha$	CO_2 captured (t/d)	[41,42]
Air separation unit	$0.01980 \cdot \alpha$	O_2 produced (t/d)	[43]
Solar			
PV panels	$0.22803 \cdot \alpha$	Power (MW)	[44]
Batteries	$500 \cdot 10^{-6} \cdot \alpha$	Battery size (kWh)	[45]
Electrolysis	$650 \cdot 10^{-6} \cdot \alpha$	Power (kW)	[46]
H_2 storage			
H_2 storage tank	$563 \cdot 10^{-6} \cdot \alpha$	H_2 mass (kg_{H2})	[47]
H_2 compressor	$0.267 \cdot (\alpha/445)^{0.67}$	Power (kW)	[48]
Pyrolysis plant	$0.65609 \cdot \alpha$	Biomass consumption (t/h)	[49]
Methanation			
CO_2 compressor	$0.267 \cdot (\alpha/445)^{0.67}$	Power (kW)	[48]
Reactors	$300 \cdot 10^{-6} \cdot \alpha$	SNG power (kW_{SNG})	[50]
Catalyst	$0.1875 \cdot \alpha$	Volume of catalyst (m^3)	[48]
Shaft bustle pipe	$0.06 \cdot \alpha$	Shaft injection (kg/t_{HM})	–
Other direct costs			
Installation	$7\% \cdot \alpha$	CAPEX (M€)	[51]
Instrumentation & control	$5\% \cdot \alpha$	CAPEX (M€)	[51]
Piping	$8\% \cdot \alpha$	CAPEX (M€)	[51]
Electrical	$4\% \cdot \alpha$	CAPEX (M€)	[51]
Building	$8\% \cdot \alpha$	CAPEX (M€)	[51]
Yard improvements	$2\% \cdot \alpha$	CAPEX (M€)	[51]
Service facilities	$11\% \cdot \alpha$	CAPEX (M€)	[51]
Land	$1\% \cdot \alpha$	CAPEX (M€)	[51]
Indirect costs			
Engineering	$6\% \cdot \alpha$	CAPEX (M€)	[51]
Legal expenses	$1\% \cdot \alpha$	CAPEX (M€)	[51]
Construction expenses	$8\% \cdot \alpha$	CAPEX (M€)	[51]
Contingency	$6\% \cdot \alpha$	CAPEX (M€)	[51]
OPEX (M€/y)			
Amine renovation	$1.1236 \cdot 10^{-4} \cdot \alpha$	CO_2 captured (t/d)	[52]
Catalyst renovation	$15\% \cdot \alpha$	Initial catalyst cost (M€)	[40]
Electricity	$10^{-6} \cdot \alpha \cdot \beta$	Electricity cost (€/MWh), Electricity purchased (MWh/y)	–
Water	$1.47 \cdot 10^{-6} \cdot \alpha$	Water consumption (m^3/y)	[53]
Biomass	$51.76 \cdot 10^{-6} \cdot \alpha$	Biomass consumption (t/y)	[54]
CO_2 transport & storage	$60 \cdot 10^{-6} \cdot \alpha$	CO_2 stored (t/y)	[55]
O&M	$3\% \cdot \alpha$	Total CAPEX (M€)	[56]
INCOMES (M€/y)			
Saved pulverized coal	$178.4 \cdot 10^{-6} \cdot \alpha$	PCI saved (t/y)	[57]
Saved fossil natural gas	$32.5 \cdot 10^{-6} \cdot \alpha$	NG saved (MWh/y)	[58]
Green premium (Steel)	$10^{-6} \cdot \alpha \cdot \beta$	Zero-emissions steel (t/y), premium tariff (€/t)	–
CO_2 tax	$10^{-6} \cdot \alpha \cdot \beta$	CO_2 avoided (t/y), CO_2 tax (€/t)	–

These batteries processed 34.2 GWh, which lead to the recovery of 29.1 GWh of electricity after accounting losses (yearly-average charge of 13.8%).

The size of the electrolyzer was determined by constrained maximization of the energy stored at nominal load, W_e^* (Fig. 7). The electrolyzer capacity was 64.2 MW. The percentage of energy processed at nominal load, with respect to the total energy processed by the electrolyzer, was 61.4%. This point corresponds to a steeper change in the slope of the curve of Fig. 7 (right), beyond which the percentage of energy stored at nominal load decreases faster.

The 90% of the PV electricity was used in the electrolyzer (Fig. 8), and the rest for O_2 production in the ASU (which is necessary for the OBF). The yearly H_2 production was 37 million Nm^3. The capacity factor of the electrolysis was 29.6% (2596 equivalent operating hours). Consequently, the electrolyzer could triple its hydrogen production by utilizing grid electricity or surplus power derived from the facility's flue

Table 7
Location and technical data of the PV solar field and electrolyzer.

System / Parameter	Value
PV panels	
Solar area (m^2)	938,889
Average system loss* (%)	35.6
Peak power (MWp)	140.8
Max. power production (MW)	120.2
Electricity production (MWh/y)	184,981
Equivalent operating hours (h)	1,313
Li-ion battery	
Round-trip efficiency (%)	85.0
Power capacity (MW)	7.04
Energy capacity (in time) (h)	4
Electricity processed (MWh/y)	34,239
Electricity provided (MWh/y)	29,103
Average charge (%)	13.8
Electrolyzer	
Consumption (kWh/Nm^3)	4.50
Power capacity (MW)	64.2
Nominal H_2 production (Nm^3/h)	14,256
Nominal O_2 production (Nm^3/h)	7,128
Usage of PV electricity (%)	90.0
Electricity processed (MWh/y)	166,535
H_2 production (Nm^3/y)	37,007,755
O_2 production (Nm^3/y)	18,503,877
Equivalent operating hours (h)	2,596
Average capacity factor (%)	29.6
Average H_2 production (Nm^3/h)	4,225

* Including effects related to the angle of incidence and temperature.

gases. However, this study focuses exclusively on the utilization of electricity derived from the facility's photovoltaic panels for the methanation integration.

4.2. Synthetic natural gas and charcoal production

Once the operation of the electrolyzer is known, the methanation plant can be sized as described in the methodology section. A small methanation size allows for a higher capacity factor, but it increases the H_2 tank that is needed for buffering. Therefore, we minimized the methanation plant size constrained by a maximum reasonable H_2 tank size of 66,740 Nm^3. Under this condition, the nominal consumption of the methanation plant was 6,656 Nm^3/h of hydrogen (i.e., 20 MW_{H2}) and 5,762 Nm^3/h of syngas (Table 8). Despite the high capacity factor in the methanation plant (63.5%, corresponding to 5,560 equivalent

Table 8
Location and technical data of the methanation and pyrolysis plant.

System / Parameter	Value
H_2 tank	
Maximum capacity (Nm^3)	66,740
Yearly average capacity (%)	23.1
Methanation	
Nominal H_2 consumption (Nm^3/h)	6,656
Nominal syngas consumption (Nm^3/h)	5,762
Nominal SNG production (Nm^3/h)	3,635
Gas conversion efficiency, ϵ (Nm^3_{SNG}/Nm^3_{H2})	0.5461
Specific syngas consumption, ν (Nm^3_{syngas}/Nm^3_{SNG})	1.5853
Equivalent operating hours (h)	5,560
Average capacity factor (%)	63.5
Yearly SNG production (Nm^3/y)	20,209,935
Pyrolysis plant	
Nominal syngas production (Nm^3/h)	5,762
Nominal charcoal production (kg/h)	2,086
Biomass consumption (kg/h)	8,584
Equivalent operating hours (h)	5,581
Average capacity factor (h)	63.7
Syngas tank	
Maximum capacity (Nm^3)	150,000
Yearly average capacity (%)	43.9

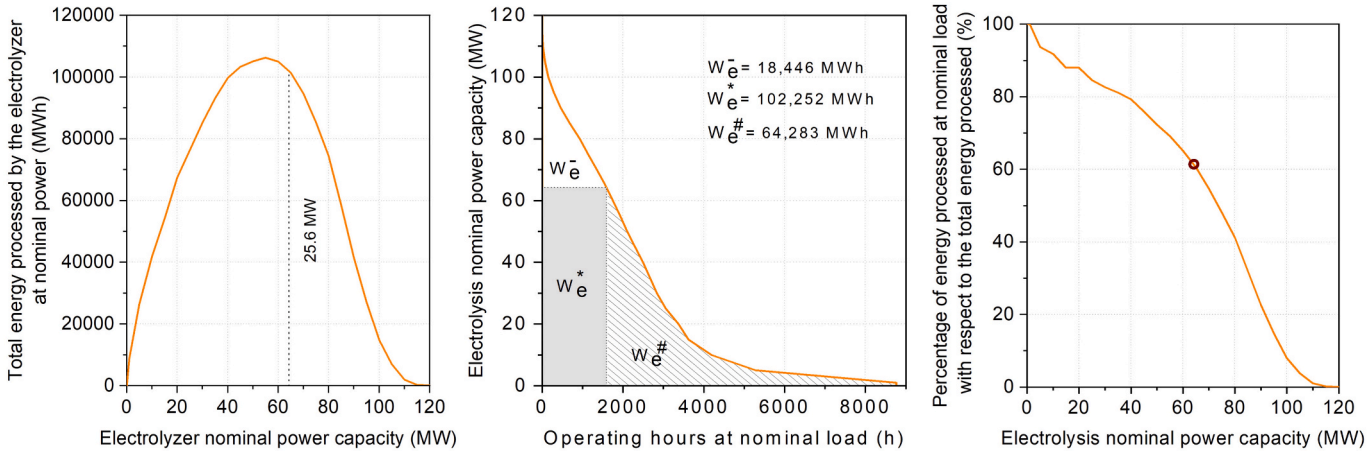

Fig. 7. Sizing of the electrolyzer.

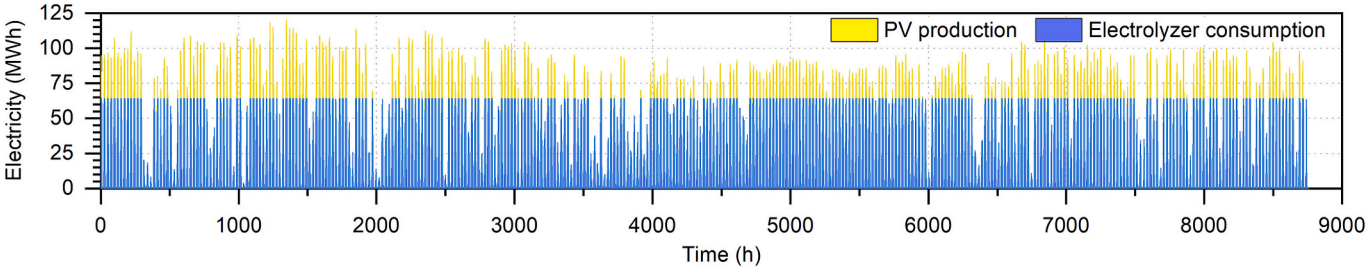

Fig. 8. PV electricity production and Electrolysis electricity consumption vs. time.

operating hours), its operation presents daily start-stop cycling (Fig. 9). The H_2 tank only facilitates shifting surplus production from midday to the evening of the same day (Fig. 10). Since hydrogen shortages typically last six hours or less, this could be mitigated by increasing electrolyzer output during these windows, either by utilizing plant surplus or purchasing grid power. In any case, this study will focus exclusively on utilizing PV-generated electricity for hydrogen production.

Since the pyrolysis plant is less flexible than the methanation plant, efforts have been focused on minimizing its downtime (Fig. 11). A 150,000 Nm^3 syngas storage tank at atmospheric pressure (typical for buffering gases in steelworks) was assumed for this case (Fig. 12). This ensures the methanation plant has a continuous syngas supply whenever operational. In practice, both plants share similar operating hours and average capacity factors (Table 8), as the pyrolysis plant is operated solely to meet methanation demand. While their shutdown profiles differ due to the larger syngas tank, both systems are sized to balance syngas supply and demand throughout the year. In practice, the pyrolysis plant is assumed to operate strictly between 80% and 100% load, with full capacity required only during start-up procedures.

The reliance on on-site PV generation introduces significant operational dynamics. Daily start-stop cycles in the methanation and pyrolysis units can lead to thermal fatigue and accelerated catalyst deactivation. To mitigate this, the proposed system architecture should assume a 'hot standby' strategy, where reactors are maintained at a minimum threshold temperature during nocturnal periods. While this prevents extreme thermal cycling, it slightly increases the internal energy demand, a factor that should be optimized in future dynamic simulations, and that could be covered with surplus off gases from the steel plant. For pyrolysis, the unit is assumed to have sufficient thermal inertia to decouple its operation from the variability.

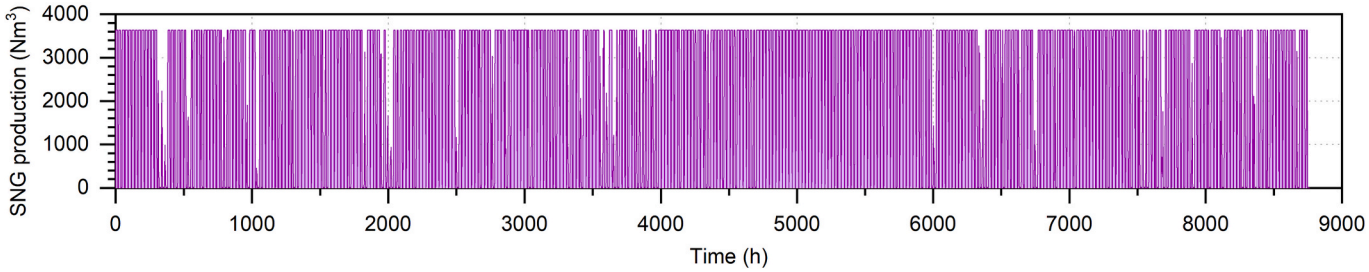

Fig. 9. Synthetic natural gas produced vs. time.

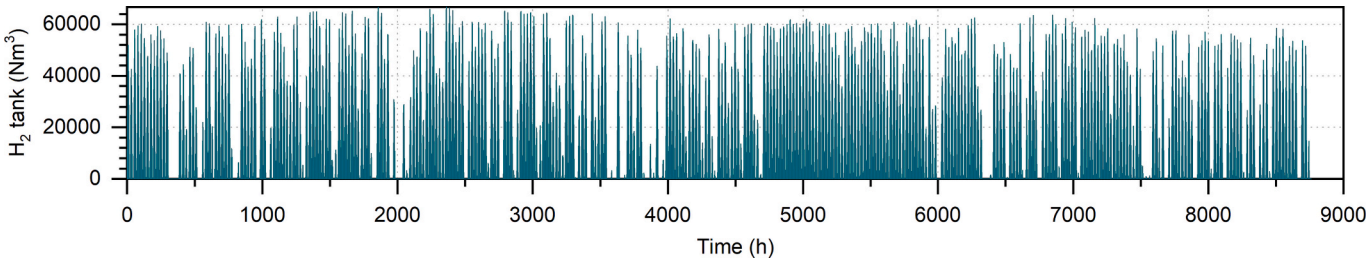

Fig. 10. H_2 stored in the tank vs. time.

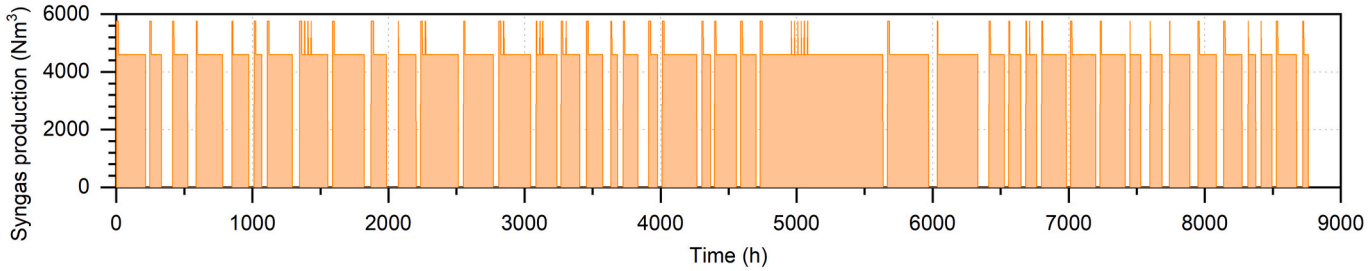

Fig. 11. Syngas produced vs. time.

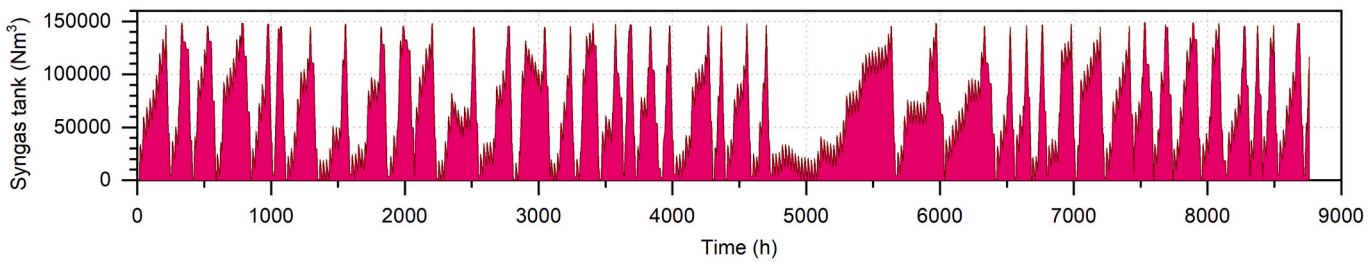

Fig. 12. Syngas stored in the tank vs. time.

Table 9
Mass flows (kg/t_{HM}) of the process flow diagrams of Fig. 2 for air-blown blast furnace and for OBF-TGR with charcoal and SNG. Results from Aspen Plus simulation. *H and O accounts for fuel moisture.

Material	T (°C)	Total	C	H	O	N	S	Fe_2O_3	FeO	Fe_3Si	Fe	Al_2O_3	SiO_2	CaO	CaS	MgO	MnO	Mn	CH_4	C_2H_4	C_2H_6	CO	CO_2	H_2	O_2	H_2O	N_2
Air-blown BF																											
Iron ore	25	1,594	–	–	–	–	–	1,272	67.0	–	–	122.7	84.6	27.5	–	16.5	3.7	–	–	–	–	–	–	–	–	–	–
Coke	25	318.2	284.4	–	–	–	–	1.9	–	–	–	10.3	20.3	0.9	–	0.4	0.0	–	–	–	–	–	–	–	–	–	–
Coal*	25	213.0	170.3	7.7	9.7	5.1	0.0	–	–	–	–	8.3	11.5	0.4	–	–	–	–	–	–	–	–	–	–	–	–	–
Air	1179	1,181	–	–	–	–	–	–	–	–	–	–	–	–	–	–	–	–	–	–	–	–	–	–	270.8	18.2	891.8
O_2	25	113	–	–	–	–	–	–	–	–	–	–	–	–	–	–	–	–	–	–	–	–	–	–	113.0	–	–
Hot metal	1510	1,000	49.3	–	–	–	–	–	–	34.9	913.3	–	–	–	–	–	–	2.5	–	–	–	–	–	–	–	–	–
Slag	1550	293.1	–	–	–	–	–	–	–	–	–	141.3	105.6	28.7	0.1	16.9	0.5	–	–	–	–	–	–	–	–	–	–
BFG	155	2,126	–	–	–	–	–	–	–	–	–	–	–	–	–	–	–	–	–	–	–	506.3	689.9	6.8	–	26.1	896.9
OBF-TGR																											
Iron ore	25	1,595	–	–	–	–	–	1,273	67.0	–	–	122.7	84.6	27.5	–	16.5	3.7	–	–	–	–	–	–	–	–	–	–
Coke	25	196.6	175.7	–	–	–	–	1.2	–	–	–	6.3	12.5	0.5	–	0.2	0.0	–	–	–	–	–	–	–	–	–	–
NG	25	52.7	–	–	–	–	–	–	–	–	–	–	–	–	–	–	–	–	52.7	–	–	–	–	–	–	–	–
SNG	35	7.3	–	–	–	–	–	–	–	–	–	–	–	–	–	–	–	–	7.2	–	–	–	0.0	0.0	–	0.1	–
Coal*	25	207.8	166.1	7.5	9.4	5.0	0.0	–	–	–	–	8.1	11.2	0.4	–	–	–	–	–	–	–	–	–	–	–	–	–
Charcoal*	25	5.2	4.8	0.0	0.1	0.0	–	–	–	–	–	0.1	0.1	0.0	–	–	–	–	–	–	–	–	–	–	–	–	–
O_2	25	416.0	–	–	–	–	–	–	–	–	–	–	–	–	–	–	–	–	–	–	–	–	–	–	414.8	0.0	1.1
Air	–	–	–	–	–	–	–	–	–	–	–	–	–	–	–	–	–	–	–	–	–	–	–	–	–	–	–
Treated BFG	800	500.0	–	–	–	–	–	–	–	–	–	–	–	–	–	–	–	–	–	–	–	427.7	48.1	15.6	–	–	8.6
Hot metal	1510	1,000	49.3	–	–	–	–	–	–	34.9	913.3	–	–	–	–	–	–	2.5	–	–	–	–	–	–	–	–	–
Slag	1550	280.8	–	–	–	–	–	–	–	–	–	137.3	97.8	28.4	0.0	16.8	0.5	–	–	–	–	–	–	–	–	–	–
BFG	137	1,700	–	–	–	–	–	–	–	–	–	–	–	–	–	–	–	–	–	–	–	732.5	823.2	26.8	–	102.6	14.7
BFG (Atm.)	137	707.3	–	–	–	–	–	–	–	–	–	–	–	–	–	–	–	–	–	–	–	304.8	342.5	11.2	–	42.7	6.1
CO_2 (CC)	35	432.6	–	–	–	–	–	–	–	–	–	–	–	–	–	–	–	–	–	–	–	–	432.6	–	–	–	–
H_2O (CC)	35	59.9	–	–	–	–	–	–	–	–	–	–	–	–	–	–	–	–	–	–	–	–	–	–	–	59.9	–
Syngas	25	13.6	–	–	–	–	–	–	–	–	–	–	–	–	–	–	–	–	1.7	0.1	0.1	5.9	5.2	0.6	–	–	–
H_2 (meth.)	25	1.7	–	–	–	–	–	–	–	–	–	–	–	–	–	–	–	–	–	–	–	–	–	1.7	–	–	–
H_2O (meth.)	50	8.0	–	–	–	–	–	–	–	–	–	–	–	–	–	–	–	–	–	–	–	–	–	–	–	8.0	–

4.3. CO_2 emissions

To quantify CO_2 emissions, we utilize the Aspen Plus blast furnace simulation. In this case, Top Gas Recycling is adjusted to maintain a constant injection of 500 kg/t_{HM} into the shaft (this keeps the percentage of direct reduction inside the furnace around 10%). Additionally, 60 kg/t_{HM} of natural gas is injected via tuyeres to control the adiabatic flame temperature (at 2190 °C), which would otherwise be excessive under oxy-fuel operation. The top gas temperature was maintained in the range of 130–140 °C, which is achieved by assuming a hydrogen utilization efficiency of 30%, consistent with industrial benchmarks for OBF-TGR systems. This configuration reduces the coke consumption close to the technical minimum of 190 kg/t_{HM} (Table 9), so no further shaft injection or tuyere injection is recommended.

The studied case aims for replacing the fossil auxiliary fuels injected in the tuyeres by carbon–neutral fuels (pulverized coal by charcoal, and natural gas by SNG). Depending on the time of the year, the extent of fuel replacement is different. In Table 9, the results for the most common case are provided, in which pyrolysis is operating at 80% load (1,668 kg/h of charcoal production) and methanation is operating at full load (2,336 kg/h of SNG production). Due to the similarities between the original and replacement fuels, and due to the low substitution rate, furnace operation remains largely unaffected despite of the replacement (adiabatic flame temperature only increases by 7 °C at most). The primary change lies in the net emission balance, as a portion of emissions now originates from biomass and can thus be considered carbon–neutral.

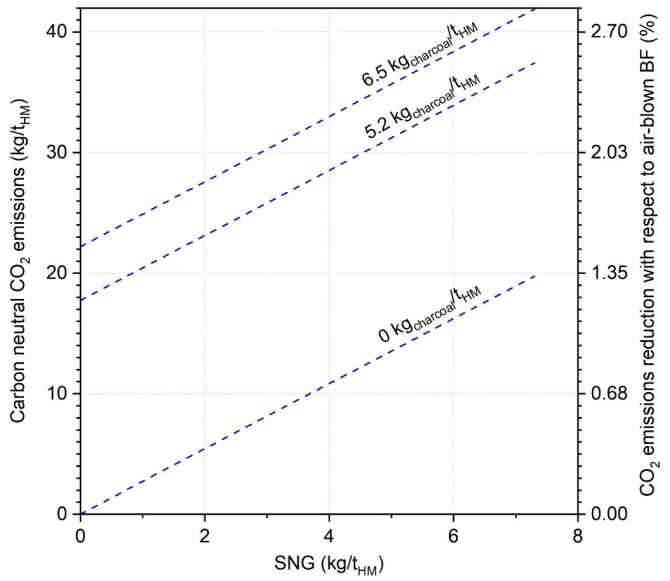

Fig. 13. Carbon-neutral CO_2 emissions as a function of charcoal and SNG replacing fossil fuel in OBF-TGR of 320 t_{HM}/h size.

The availability of these replacement fuels is independent. Charcoal is sourced directly from the pyrolysis plant (which operates more continuously than the methanation unit) and is consumed as it is produced. Conversely, SNG production depends on H_2 availability, fluctuating daily. The resulting neutral emissions for a blast furnace producing 320 t_{HM}/h are shown in Fig. 13 for different fuel replacements. In the case of coal, replacement may reach the 3% temporarily, while for natural gas the replacement may rise to 12% at some hours. This replacement is notably limited, and not always taking place, as it is constrained by the H_2 available for methanation. This availability is, in turn, dictated by the PV installation area, which ultimately determines also the volume of biomass to pyrolyze.

When comparing the studied case with conventional air-blown blast furnace, the CO_2 reductions come through multiple pathways. First, operating in OBF-TGR mode yields a 15.4 percentage point reduction. Furthermore, if the CO_2 captured during TGR were permanently stored, emissions would decrease by an additional 29.2 percentage points. Finally, an extra 1.8 percentage point reduction is achieved using charcoal and SNG during the year, limited by the capacity of the PV panels (green band in Fig. 14). Readers should note that the scope of this paper is specifically to evaluate the extent to which this integration can be achieved using only electricity generated on-site (rooftop PV). This does not imply that a full substitution of natural gas and pulverized coal is impractical, provided sufficient hydrogen and biomass are available (a scenario which, as noted in the introduction, theoretically yields CO_2 reductions of up to 70%).

4.4. Levelized cost of CO_2 avoided and green premium for net-zero steel

This economic analysis quantifies the additional cost of an OBF-TGR

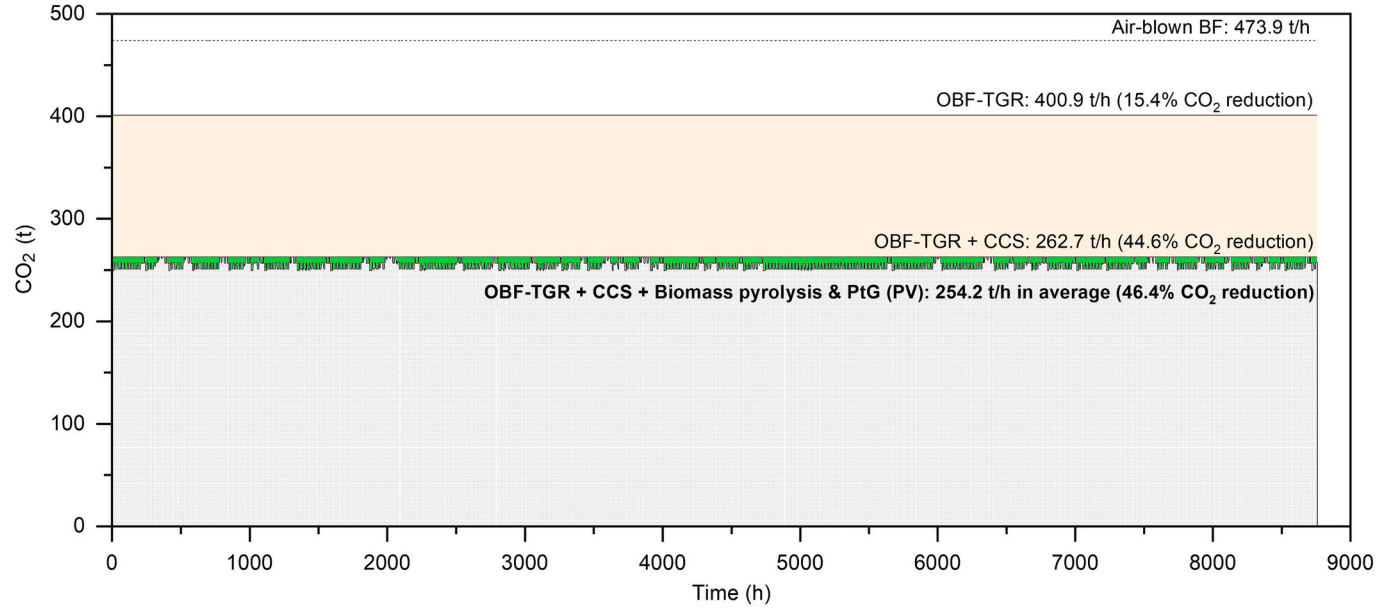

Fig. 14. Blast furnace CO_2 emissions vs. time (BF producing 320 t_{HM}/h).

Table 10
Results of the economic analysis for BOF-TGR with charcoal and PtG (PV). Electricity price: 70 €/MWh; CO_2 tax: 70 €/t_{CO2}; Green premium (steel): 150 €/t.

Parameter	Value
CAPEX (M€)	
CO_2 capture & storage plant	225.0
Air separation unit	63.3
PV panels	32.1
Batteries for PV panels	14.1
Electrolysis	41.7
H_2 tank	3.4
H_2 compressor	0.3
Pyrolysis plant	5.6
Syngas compressor	0.2
Methanation reactors	9.6
Methanation catalyst	9.5
Shaft injection bustle pipe	30.0
Other direct cost: Installation	92.2
Other direct cost: Instrumentation & control	65.9
Other direct cost: Piping	105.4
Other direct cost: Electrical	52.7
Other direct cost: Building	105.4
Other direct cost: Yard improvements	26.4
Other direct cost: Service facilities	144.9
Other direct cost: Land	13.2
Indirect cost: Engineering and supervision	79.1
Indirect cost: Legal expenses	13.2
Indirect cost: Construction expenses	105.4
Indirect cost: Contingency	79.1
Total:	1317.7
OPEX (M€/y)	
Amine renovation	0.4
Catalyst renovation	1.4
Electricity (for ASU)	29.7
Water	0.0
Biomass	2.5
CO_2 transport & storage	72.7
O&M	39.5
Total:	146.3
INCOMES (M€/y)	
Saved PCI	2.1
Saved NG	7.6
Green premium (steel)	195.1
Saved CO_2 tax	134.7
Total:	339.5

compared to a conventional blast furnace, and evaluates offsetting this cost through green steel premiums and CO_2 tax savings. The savings in replacing fossil fuel are notably lower due to the small replacement ratio, which is limited by the PV capacity. The total CAPEX is 1,318 M€, driven mainly by the CO_2 capture and storage process, followed by the electrolyzer, PV and shaft bustle pipe. The total equipment cost represents 33% of total CAPEX.

Regarding the OPEX, the two major contributors are the cost associated to CO_2 transport and storage, and the electricity for the ASU. For the latter, we used the unused PV electricity (10% of total PV production), but it only represented the 4.2% of the total ASU's electricity consumption (at 380 kWh/t_{O2} [59]). In the OPEX, the cost of the electricity purchased from the grid was set at 70 €/MWh, the cost of biomass at 51.8 €/t [54], and the cost of CO_2 transport & storage at 60 €/t [55].

Regarding the incomes, the save PCI was quantified at 178.4 €/t [57] and the NG at 32.5 €/MWh [58]. For the data presented in Table 10, the green premium for net-zero steel was 150 €/t, and the CO_2 tax 70 €/t. Under this favorable scenario, the integration is profitable. The reader should note that although the overall emission reduction is partial, the avoided carbon can be aggregated annually to certify 46.4% of the output as net-zero steel. This approach assigns the total CO_2 avoided by the integrated plant to an equivalent fraction of the final steel output. This linear attribution is consistent with the 'mass balance' chain of custody defined in ISO 14067. The remaining tonnage is classified as residual production with an emission profile consistent with a conventional air-blown blast furnace. Consequently, the green premium is applied only to the certified batch.

Additionally, some sensitivity analyses were performed over the green premium and the CO_2 tax (Fig. 15). In Japan, for instance, the carbon market is still emerging with prices around 5 €/t_{CO2}. Without significant carbon tax savings, a green premium of 186 €/t would be required to achieve profitability (a figure well within current market expectations for green steel). At carbon prices of 50 €/t, the necessary green premium drops to 112 €/t. Since both scenarios align with current market trends, OBF-TGR stands as a commercially viable decarbonization pathway for the steel industry. This specific study integrated biomass and methanation; however, given their marginal contribution to total CO_2 reduction, it is difficult to isolate their specific impact on these economic outcomes.

Finally, the Levelized Cost of CO_2 Avoidance (LCCA) (i.e., the carbon tax rate required to achieve a cumulative NPV of zero) was analyzed

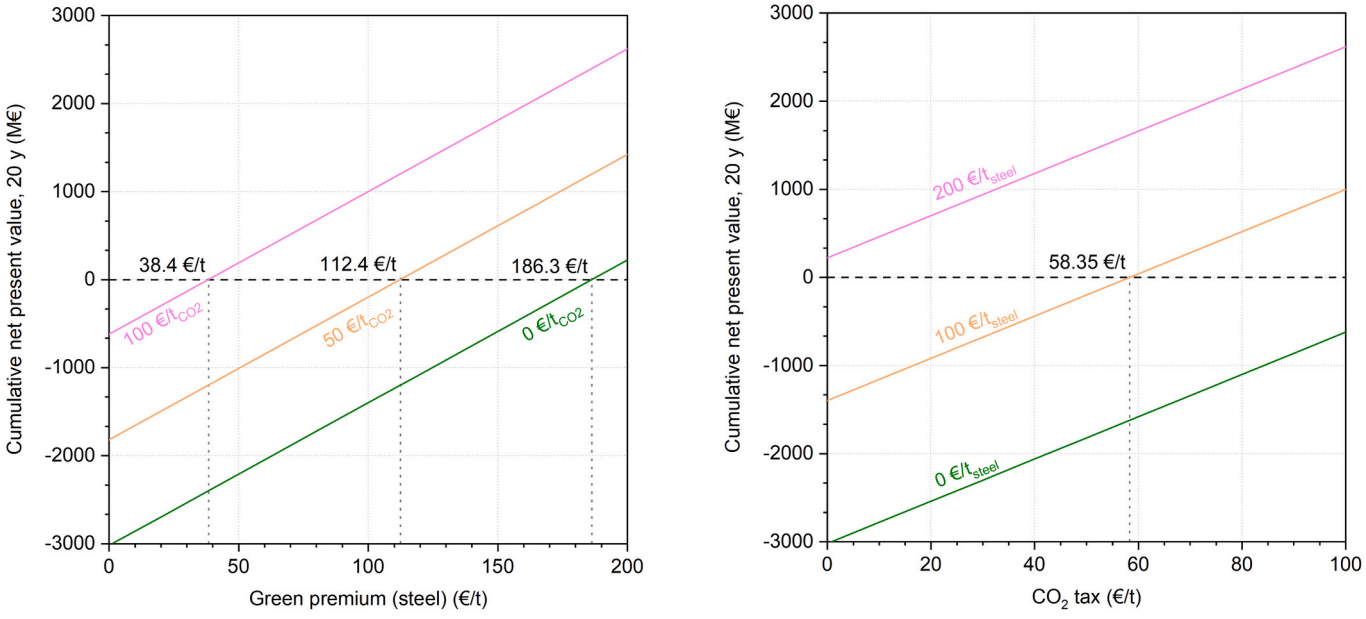

Fig. 15. Cumulative net present value, 20 years (M€). Sensitivity analysis on Green premium for net-zero steel (€/t) and CO_2 tax (€/t).

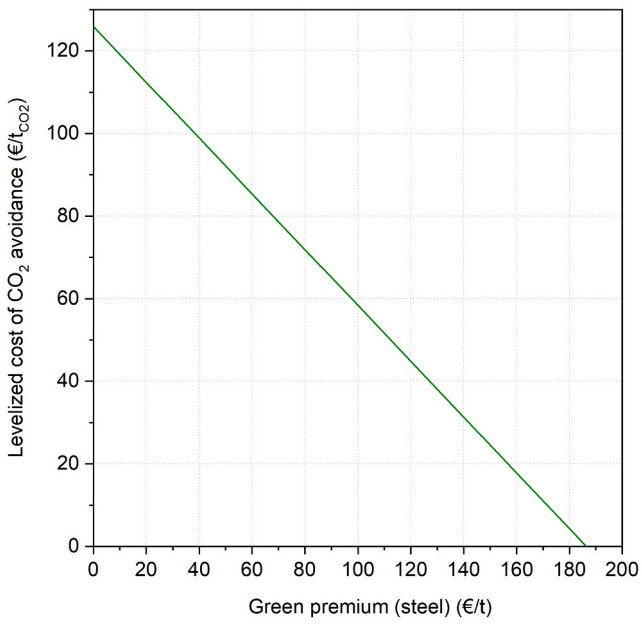

Fig. 16. Levelized cost of CO_2 avoidance (€/t_{CO2}) vs. Green premium for net-zero steel (€/t).

relative to the green steel premium for the OBF-TGR (Fig. 16). Fig. 16 provides a direct calculation of the 'break-even' point for any combination of market premiums and regulatory carbon costs, demonstrating the conditions under which the OBF-TGR-PtG-Biomass integration remains commercially viable. The LCCA starts at 125.9 €/t_{CO2} with no premium and decreases linearly to zero at a green premium of 186 €/t steel.

While the CAPEX of the ASU, electrolyzers, and PV system constitutes a relevant part of the initial investment, these parameters were not included in the sensitivity analysis. The rationale is that the system's scale is physically capped by the available rooftop area (141 MWp). Unlike unconstrained projects where a drop in technology costs might lead to larger installations, in this case study, the technical configuration remains static. Consequently, the economic feasibility is much more sensitive to external market incentives, such as CO_2 taxes and the Green Steel Premium, than to the capital cost of the equipment itself.

Despite the promising results, this study has certain limitations that define its scope. First, the rooftop area constraint represents a physical ceiling for on-site decarbonization; however, future work could explore the integration of off-site power purchase agreements to supplement this capacity. Second, the model assumes a constant top gas recycling rate, whereas in a real industrial environment, this could be dynamically adjusted based on gas quality and furnace stability. Third, the absence of grid interaction was a deliberate choice to assess maximum self-sufficiency, but hybrid operations (grid + PV) could potentially lower the levelized cost of CO_2 avoidance by increasing the electrolyzer's capacity factor. These factors represent the next steps in refining the techno-economic assessment of integrated OBF-TGR-PtG systems.

5. Conclusions

Innovative methods for CO_2 reduction in blast furnaces are still under development. Oxygen Blast Furnaces and their various integrations represent one of the most promising pathways. Literature suggests the highest emission reduction potential lies in integrating OBF with Top Gas Recycling, pyrolyzed biomass, and syngas methanation. This study analyzes the practical viability of this integration when powered by on-site rooftop PV systems. The JFE Steel plant in Chiba, Japan, serves as the case study for this research. Renewable resource management is governed by an hourly decision-making methodology that utilizes load operating curves to maximize the electrolyzer's full-load energy consumption from rooftop PV. The blast furnace was modeled in Aspen Plus using the extended operating line approach. Finally, the economic feasibility was assessed via a 'factored estimate' methodology based on major equipment costs, providing an accuracy of ±30%.

The available roof area for PV installation was determined by classifying structures via visual inspection in Google Earth. Type 1 roofs are immediately suitable for installation, with minimal interference from shading or dust. Type 2 roofs require structural rehabilitation or dust mitigation, necessitating additional capital expenditure. For this study, the scope was limited strictly to Type 1 surfaces. These primary roofs cover 0.94 km^2, providing a peak capacity of 141 MWp. This configuration yields an annual electricity production of 185 GWh (1,310 equivalent operating hours). With a selected electrolyzer capacity of 64 MW, approximately 90% of the generated power is directly utilized, resulting in an annual green hydrogen yield of 37 million Nm^3 at a 30% capacity factor.

The methanation plant was optimized for a maximum H_2 storage of 66.700 Nm^3. This setup results in a nominal hydrogen consumption of 6,660 Nm^3/h and a 63% capacity factor. Despite the storage, the plant still undergoes near-daily start-stop cycles. The pyrolysis plant uses a larger 150,000 Nm^3 storage due to its lower flexibility. In practice, both plants share similar operating hours because the pyrolysis unit runs strictly to meet methanation syngas demand. The pyrolysis unit consumes 8.6 t/h of biomass to produce 5,760 Nm^3/h of syngas and 2.1 t/h of charcoal.

Compared to a conventional air-blown blast furnace (1481 kg_{CO2}/t_{HM}), the studied case achieves CO_2 reductions through three primary drivers: transitioning to OBF-TGR mode provides an initial 15.4 percentage point decrease, while permanently storing the captured CO_2 adds a further 29.2 percentage point reduction. An additional 1.8 percentage point saving is realized by integrating charcoal and SNG, a figure currently scaled to the year-round capacity of the supporting PV infrastructure. In practice, while this integration could potentially reduce emissions by 65–70% with unlimited renewable energy, the actual reduction is capped at 46.4% when syngas methanation relies solely on rooftop PV electricity. This demonstrates that total self-sufficiency is unattainable under PtG integrations; consequently, emission savings remain largely dependent on OBF and TGR contributions, aligning well with literature benchmarks of 10–40% depending on whether CO_2 is stored. Consequently, unless off-site renewable energy is sourced, a simplified OBF-TGR configuration is recommended as the most cost-effective and immediate decarbonization strategy for existing steel plants.

The economic analysis confirms that while the OBF-TGR integration involves a significant CAPEX of 1,320 M€ (driven primarily by carbon capture and electrolytic processes), the system achieves commercial viability under current market trends. Although the 46.4% emission reduction is partial, it allows for the certification of a proportional batch of net-zero steel, making the project profitable through a combination of green premiums and CO_2 tax savings. Sensitivity analysis reveals a Levelized Cost of CO_2 Avoidance starting at 126 €/t_{CO2}, which can be fully offset if green steel premiums reach 186 €/t. Ultimately, despite the limited contribution of biomass and methanation due to PV constraints, the OBF-TGR pathway stands as a robust and financially feasible decarbonization strategy for the steel industry.

This study also highlights the role of industrial symbiosis through biomass integration, showing how regional bio-waste can be valorized as a reducing agent in the steelmaking process. Future work could apply this PV-constrained model to different geographic regions to quantify how local solar irradiance and regional biomass availability dictate the decarbonization limits of the OBF-TGR-PtG route. Finally, it is important to acknowledge the boundaries of the present study. This research focuses on the direct operational CO_2 emissions of the integrated steel plant. Future work should also expand this analysis into a full Life Cycle Assessment to account for the embodied carbon emissions associated

with the manufacturing of photovoltaic panels and large-scale battery systems, as well as the carbon footprint of biomass collection and transportation. These factors will be essential to further refine the net decarbonization potential of the OBF-TGR-PtG route as the technology moves toward commercial maturity.

CRediT authorship contribution statement

Manuel Bailera: Writing – original draft, Visualization, Validation, Software, Methodology, Investigation, Funding acquisition, Formal analysis, Conceptualization. **Alexander García-Mariaca:** Writing – original draft, Validation, Investigation, Formal analysis.

Declaration of competing interest

The authors declare that they have no known competing financial interests or personal relationships that could have appeared to influence the work reported in this paper.

Acknowledgments

This publication is supported by RYC2022-038283-I, funded by MCIN/AEI/10.13039/501100011033 and the European Social Fund Plus (ESF+). This article is part of the R&D project PID2023-149968OB-I00, funded by MICIU/AEI/10.13039/501100011033/ and by FEDER, UE. Aspen Technology Inc is also acknowledged for the use of the software.

Data availability

Data will be made available on request.

References

[1] International Energy Agency, Iron and Steel Technology Roadmap. 2020.
[2] Midrex Technologies, 2022. The Midrex (R) Process. n.d.
[3] Bene C, Mahmoud M, Opinska LG, Rademaekers K. Moving Towards Zero-Emission Steel 2021:46.
[4] Perpiñán J, Peña B, Bailera M, Eveloy V, Kannan P, Raj A, et al. Integration of carbon capture technologies in blast furnace based steel making: a comprehensive and systematic review. Fuel 2023;336:127074. https://doi.org/10.1016/j.fuel.2022.127074.
[5] von Scheele J. Decarbonization of ironmaking. MM Steel Club 2021.
[6] Sato M, Takahashi K, Nouchi T, Ariyama T. Predictcion of next-generation ironmaking process based on oxygen blast furnace suitable for CO2 mitigation and energy flexibility. ISIJ Int 2015;55:2105–14. https://doi.org/10.2355/isijinternational.ISIJINT-2015-264.
[7] Quader MA, Ahmed S, Raja Ghazilla RA, Ahmed S, Dahari M. Evaluation of criteria for CO2 capture and storage in the iron and steel industry using the 2-tuple DEMATEL technique. J Clean Prod 2016;120:207–20. https://doi.org/10.1016/j.jclepro.2015.10.056.
[8] Zhang W, Zhang J, Xue Z, Zou Z, Qi Y. Unsteady analyses of the top gas recycling oxygen blast furnace. ISIJ Int 2016;56:1358–67. https://doi.org/10.2355/isijinternational.ISIJINT-2016-090.
[9] Ariyama T, Sato M, Nouchi T, Takahashi K. Evolution of blast furnace process toward reductant flexibility and carbon dioxide mitigation in steel works. ISIJ Int 2016;56:1681–96. https://doi.org/10.2355/isijinternational.ISIJINT-2016-210.
[10] She X, An X, Wang J, Xue Q, Kong L. Numerical analysis of carbon saving potential in a top gas recycling oxygen blast furnace. J Iron Steel Res Int 2017;24:608–16. https://doi.org/10.1016/S1006-706X(17)30092-4.
[11] Wang H, Chu M, Guo T, Zhao W, Feng C, Liu Z, et al. Mathematical simulation on blast furnace operation of coke oven gas injection in combination with top gas recycling. Steel Res Int 2016;87:539–49. https://doi.org/10.1002/srin.201500372.
[12] Bailera M, Nakagaki T, Kataoka R. Revisiting the Rist diagram for predicting operating conditions in blast furnaces with multiple injections. Open Res Europe 2021;1. https://doi.org/10.12688/openreseurope.14275.1.
[13] Pascual S, Bailera M, Perpiñán J, Lisbona P. CO2 conversion to methane. Advances and technology development in greenhouse gases: emission, capture and conversion. Elsevier; 2024. p. 165–93. https://doi.org/10.1016/B978-0-443-19235-7.00019-1.
[14] Faria DG, Carvalho MMO, Neto MRV, de Paula EC, Cardoso M, Vakkilainen EK. Integrating oxy-fuel combustion and power-to-gas in the cement industry: a process modeling and simulation study. Int J Greenhouse Gas Control 2022;114:103602. https://doi.org/10.1016/j.ijggc.2022.103602.
[15] Bailera M, Rebolledo B. Integration of power to gas and biomass charcoal in oxygen blast furnace ironmaking. Energy Convers Manag 2024;300. https://doi.org/10.1016/j.enconman.2023.117916.
[16] Tseitlin MA, Lazutkin SE, Styopin GM. A flow-chart for iron making on the basis of 100% usage of process oxygen and hot reducing gases injection. ISIJ Int 1994;34:570–3. https://doi.org/10.2355/isijinternational.34.570.
[17] Zhou Z, Yi Q, Wang R, Wang G, Ma C. Numerical investigation on coal combustion in ultralow CO2 blast furnace: effect of oxygen temperature. Processes 2020;8:877. https://doi.org/10.3390/pr8070877.
[18] Takahashi K, Nouchi T, Sato M, Ariyama T. Perspective on progressive development of oxygen blast furnace for energy saving. ISIJ Int 2015;55:1866–75. https://doi.org/10.2355/isijinternational.ISIJINT-2015-196.
[19] Arasto A, Tsupari E, Kärki J, Lilja J, Sihvonen M. Oxygen blast furnace with CO2 capture and storage at an integrated steel mill-Part I: Technical concept analysis. Int J Greenhouse Gas Control 2014;30:140–7. https://doi.org/10.1016/j.ijggc.2014.09.004.
[20] Barón C, Bailera M, Perpiñán J, Peña B. A comparison of carbon capture and biomass utilisation for decarbonising oxygen blast furnace ironmaking. Fuel 2026;409:137810. https://doi.org/10.1016/j.fuel.2025.137810.
[21] Liu Y, Shen Y. Modelling and optimisation of biomass injection in ironmaking blast furnaces. Prog Energy Combust Sci 2021;87:100952. https://doi.org/10.1016/j.pecs.2021.100952.
[22] Legaz J. Manuel Bailera. Universidad de Zaragoza, Decarbonisation of Blast Furnaces through biomass pyrolysis and Power to Gas; 2025.
[23] Feliciano-Bruzual C. Charcoal injection in blast furnaces (Bio-PCI): CO2 reduction potential and economic prospects. J Mater Res Technol 2014;3:233–43. https://doi.org/10.1016/j.jmrt.2014.06.001.
[24] Bailera M, García-Mariaca A, Barón C. Decarbonisation of lime kilns in ironmaking plants through Power to Gas. Res Eng 2026:110076. https://doi.org/10.1016/j.rineng.2026.110076.
[25] Google Earth, Imagen por satelite de JFE Steel, en Chiba, Japón (35°34'23"N, 140°05'41"E). 2024.
[26] European Commission. PVGIS ver. 5.2 2022.
[27] Center for Sustainable Systems University of Michigan. Photovoltaic energy factsheet 2021;CSS07-08.
[28] International Energy Agency. Special Report on Solar PV Global Supply Chains 2022.
[29] European Commission. Using PVGIS - Frequently Asked Questions (https://joint-research-centre.ec.europa.eu/photovoltaic-geographical-information-system-pvgis/getting-started-pvgis/using-pvgis-frequently-asked-questions_en) n.d.
[30] Iberdrola. Puertollano: Green hydrogen plant for industrial use (Infographic) 2022.
[31] National Rural Utilities Cooperative Finance Corporation. Battery Energy Storage Overview 2019.
[32] Bailera M, Lisbona P, Peña B, Romeo LM. Energy Storage. Cham: Springer International Publishing; 2020. 10.1007/978-3-030-46527-8.
[33] Bailera M, Peña B, Lisbona P, Romeo LM. Decision-making methodology for managing photovoltaic surplus electricity through Power to Gas : combined heat and power in urban buildings. Appl Energy 2018;228:1032–45. https://doi.org/10.1016/j.apenergy.2018.06.128.
[34] NEL Hydrogen. M Series Containerized Proton Exchange Membrane (PEM) Hydrogen Generation Systems 2021.
[35] Bailera M, Nakagaki T, Kataoka R. Extending the operating line methodology to consider shaft and preheating injections in blast furnaces. ISIJ Int 2022;62. https://doi.org/10.2355/isijinternational.ISIJINT-2022-111.
[36] Rist A, Meysson N. A dual graphic representation of the blast-furnace mass and heat balances. JOM 1967;19:50–9. https://doi.org/10.1007/bf03378564.
[37] Bailera M. Comparing different syngas for blast furnace ironmaking by using the extended operating line methodology. Fuel 2023;333:126533. https://doi.org/10.1016/j.fuel.2022.126533.
[38] Izumiya K, Shimada I. Methane producing technology from CO2 for carbon recycling. In: The First Symposium on Carbon Ultimate Utilization Technologies for the Global Environment; 2021. p. 34–5.
[39] Chang J, Chen K, Li J, Lin L, Hu E, Liu K, et al. Liquid amine-based CO2 capture: a review of absorbent systems innovation, multi-scenario applications, and machine learning-assisted optimization. Renew Sustain Energy Rev 2026;231:116754. https://doi.org/10.1016/j.rser.2026.116754.
[40] Bailera M, Espatolero S, Lisbona P, Romeo LM. Power to gas-electrochemical industry hybrid systems: a case study. Appl Energy 2017;202:435–46. https://doi.org/10.1016/j.apenergy.2017.05.177.
[41] Great Plains Institute (Jill Syvrud). GPI Hosts US Delegation on Steel & Carbon Capture to United Arab Emirates, Belgium, and Netherlands. Https://BetterenergyOrg/Blog/Gpi-Hosts-Us-Delegation-on-Steel-Carbon-Capture-to-United-Arab-Emirates-Belgium-and-Netherlands/#:~:Text=ADNOC%20and%20Masdar%20partnered%20to%20build%20a,Around%20800%2C000%20metric%20tons%20of%20CO2%20annually 2019.
[42] MASDAR. ADNOC and Masdar Launch Joint Venture to Develop Commercial-Scale Carbon Capture, Usage and Storage Projects. Https://MasdarAe/En/News/Newsroom/Adnoc-and-Masdar-Launch-the-Middle-Easts-First-Joint-Venture-to-Develop-Commercial-Scale-Carbon-Cap n.d.
[43] Linde. Linde Expands Agreement with Steel Authority of India Limited. Https://WwwLindeCom/News-and-Media/2024/Linde-Expands-Agreement-with-Steel-Authority-of-India-Limited 2024.
[44] IRENA. Renewable power generation costs in 2024. Abu Dhabi 2025.
[45] Lazard. LAZARD'S LEVELIZED COST OF STORAGE ANALYSIS—VERSION 5.0. 2019.
[46] Lichner C. Electrolyzer prices – what to expect. PV Magazine 2024.

[47] Ali SM, Andrews J. Low-cost storage options for solar hydrogen systems for remote area power supply. 16th World Hydrogen Energy Conference 2006, WHEC 2006 2006;2:1269–79.
[48] De Saint JM, Baurens P, Bouallou C, Couturier K. Economic assessment of a power-to-substitute-natural-gas process including high-temperature steam electrolysis. Int J Hydrogen Energy 2015;40:6487–500. https://doi.org/10.1016/j.ijhydene.2015.03.066.
[49] BESTON. Pyrolysis Plant Cost Options from Beston Group. Https://WwwBestongroupCom/Pyrolysis-Plant/Cost/ 2026.
[50] Lehner M, Tichler R, Steinmüller H, Koppe M. Power-to-Gas: Technology and Business Models. Cham: Springer International Publishing; 2014. DOI: 10.1007/978-3-319-03995-4.
[51] Peters MS, Timmerhaus KD, West RE. Plant Design and Economics for Chemical Engineers. 5th ed. McGraw-Hill; 2003.
[52] Kohl AL, Nielsen RB. Gas Purification. 1997. DOI: DOI: 10.1016/B978-0-88415-220-0.X5000-9.
[53] Benjaminsson G, Benjaminsson J, Rudberg RB. Power-to-Gas - a technical review. Svenskt Gastekniskt Center AB 2013.
[54] BOE. Resolución de 31 de diciembre de 2025, de la Secretaría de Estado de Energía, por la que se actualizan los valores de la retribución a la operación correspondientes al primer trimestre natural del año 2026 de las instalaciones tipo de generación de energía eléctrica cuyos costes de explotación dependan esencialmente del precio del combustible. 2026.
[55] Lockwood T, Ulama D. Key insights on EU CO_2 transport and storage costs from CATF's new interactive tool. Https://WwwCatfUs/2025/11/Key-Insights-Eu-Co2-Transport-and-Storage-Costs/ n.d.
[56] Abu-Zahra MRM, Niederer JPM, Feron PHM, Versteeg GF. CO2 capture from power plants. Part II. a parametric study of the economical performance based on mono-ethanolamine. Int J Greenhouse Gas Control 2007;1:135–42. https://doi.org/10.1016/S1750-5836(07)00032-1.
[57] Mysteel. PCI coal prices: China's major cities. Https://WwwMysteelNet/Price-Summary/499786-Pci-Coal-Prices-Chinas-Major-Cities n.d.
[58] Trading Economics. Natural gas EU (EUR/MWh). Https://TradingeconomicsCom/Commodity/Eu-Natural-Gas n.d.
[59] Perpiñán J, Bailera M, Peña B, Romeo LM, Eveloy V. Technical and economic assessment of iron and steelmaking decarbonization via power to gas and amine scrubbing. Energy 2023;276:127616. https://doi.org/10.1016/j.energy.2023.127616.